CERN 98-237

MPI-PhT/98-51

The PHMC algorithm for simulations of dynamical fermions: I – description and properties

Roberto Frezzotti[1] and Karl Jansen[2,*]

[1] Max-Planck-Institut für Physik, Föhringer Ring 6, D-80805 München, Germany

[2] CERN, 1211 Genève 23, Switzerland

January 8, 2014

Abstract

We give a detailed description of the so-called Polynomial Hybrid Monte Carlo (PHMC) algorithm. The effects of the correction factor, which is introduced to render the algorithm exact, are discussed, stressing their relevance for the statistical fluctuations and (almost) zero mode contributions to physical observables. We also investigate rounding-error effects and propose several ways to reduce memory requirements.

*Heisenberg foundation fellow

1 Introduction

Although lattice QCD [1] has nowadays reached a relatively mature age, precise quantitative results –at least in the full theory– are still rare. One of the main reasons is certainly that numerical simulations of lattice QCD, including the effects of dynamical quarks, are still very demanding and computer time consuming (for reviews of dynamical fermion algorithms see [2, 3]). Efforts to improve on this situation are therefore highly desirable.

In this paper we extend the discussion of the so-called Polynomial Hybrid Monte Carlo (PHMC) algorithm, which we introduced in [4] as an attempt to improve the performance of simulation algorithms for dynamical fermions.

The main idea of the PHMC algorithm relies on dividing the eigenvalue spectrum of the Wilson-Dirac operator M on the lattice into different disjoint parts. These different parts of the eigenvalue spectrum are then treated by either incorporating them in the update step of a simulation algorithm or by taking them into account in a reweighing procedure. This general idea is realized in practise by designing suitable polynomials that approximate the inverse of $M^\dagger M$, which is needed in the actual simulation, with a different accuracy for different parts of the eigenvalue spectrum of $M^\dagger M$. In the present paper we choose a polynomial approximation to the inverse of $M^\dagger M$ which is equivalent to basically neglecting the contribution of the low-lying modes and taking very precisely into account all the other modes in the update step. This choice, which follows the original suggestion in [5], is motivated by the experience with the multiboson technique [6, 7, 8, 9, 10]: neglecting in the update a small number of low-lying modes of $M^\dagger M$ still yields results very close to the ones obtained using the exact Hybrid Monte Carlo (HMC) algorithm. We want to emphasize, however, that our choice is only a special case and the general method allows for a greater flexibility including ideas like the one proposed in [11].

One may argue that the reweighing step can be replaced by a reject/accept step in order to render the algorithm exact. We think that this is not the best choice for the following reason: it is expected that almost zero modes of the Wilson-Dirac operator appear when working in large physical volumes or at large values of the lattice spacing. In such a situation a reject/accept step leads to a dilemma: either the acceptance probability becomes so small that such events are always

rejected. Or, if they are accepted, the zero modes give exceptional values to quark propagators, distorting a statistical sample substantially. However, in full QCD, gauge configurations carrying zero modes may give a finite contribution to several fermion observables, which should be taken into account –at least in principle– in order to get correct statistical averages. In fact, we consider this scenario as a potential danger for the Hybrid Monte Carlo (HMC) algorithm [12] which is commonly used.

As we will demonstrate below, with a suitable reweighing procedure, this problem can be overcome elegantly. Namely, in our way of correcting for the polynomial approximation, the reweighing factor becomes proportional to the almost zero mode and hence cancels any singularity appearing in quark propagators used to construct physical observables. This mechanism reflects in a sense the role of the determinant when the full QCD partition function is considered. Of course, reweighing techniques are widespread in applications for numerical simulations. However, we would like to point out that our implementation of the reweighing factor makes its computation very straightforward and reliable in all cases and does not give too large an overhead in a simulation.

In a previous publication [4] we introduced the PHMC algorithm and gave some first, promising results in practical applications for Wilson fermions. However, it is by now well known that when using Wilson fermions for simulations of lattice QCD, one has to face large lattice cutoff effects in physical observables. For example, the axial Ward identity can be substantially distorted in this case [13]. However the effects of a non-vanishing lattice spacing can be systematically reduced by applying Symanzik's improvement programme [14]: this turns out to be easier in practice if only on-shell quantities are to be O(a) improved [15].

In fact, implementing the improvement programme non-perturbatively for both the action and all the local operators relevant for on-shell observables, one can reach a complete cancellation of the cutoff effects that appear linear in the lattice spacing [16, 17]. Since with such an improved theory we expect to be able to work at a much larger lattice spacing, a substantial gain in the cost of numerical simulations can be obtained. Indeed, the non-perturbative on-shell O(a) improved action has by now already been computed also for dynamical fermions [18]. Any new simulation algorithm should hence have the ability to be applicable to improved fermions. We therefore extend here our tests of the PHMC algorithm to

the case of O(a) improved actions. In the present paper we are going to discuss a number of important technical aspects of the PHMC algorithm. Numerical results for the performance of the algorithm in practise are deferred to a separate publication [19].

2 The PHMC algorithm

We introduce the PHMC algorithm and discuss several aspects concerning our practical implementation of the algorithm. In particular, we derive the computational cost of the algorithm in terms of matrix times vector operations.

2.1 Introducing the PHMC algorithm

We consider Euclidean QCD with $n_f = 2$ degenerate flavours regularized on a hypercubic space-time lattice with lattice spacing a and size $L^3 \times T$. With the lattice spacing set to unity from now on, the points on the lattice have integer coordinates (t, x_1, x_2, x_3) which are in the range $0 \leq t \leq T; 0 \leq x_i < L$. A gauge field $U_\mu(x) \in SU(3)$ is assigned to the link pointing from the site x to the site $(x + \mu)$, where $\mu = 0, 1, 2, 3$ designates the 4 forward directions in space-time. Throughout the paper we will adopt Schrödinger functional boundary conditions as detailed in [20, 21, 17]. The partition function for lattice QCD with $n_f = 2$ degenerate flavours of quarks is given by

$$\mathcal{Z} = \int \mathcal{D}U e^{-S_g[U]} \det(Q^2[U]) \; , \tag{1}$$

where S_g is the standard Wilson-plaquette action for the pure gauge sector with a coupling strength $\beta = 6/g_0^2$ and g_0 the bare gauge coupling. The Hermitean matrix Q, defining the fermion action, is given by

$$\begin{aligned} Q(U)_{xy} = & \frac{c_0}{c_M}\gamma_5[(1 + \sum_{\mu\nu}[\frac{i}{2}c_{\rm sw}\kappa\sigma_{\mu\nu}\mathcal{F}_{\mu\nu}(x)])\delta_{x,y} \\ & - \kappa\sum_\mu\{(1-\gamma_\mu)U_\mu(x)\delta_{x+\mu,y} + (1+\gamma_\mu)U_\mu^\dagger(x-\mu)\delta_{x-\mu,y}\}] \; , \end{aligned} \tag{2}$$

where κ is the hopping parameter, related to the bare quark mass m_0 by $\kappa = 1/(8 + 2m_0)$ and $c_{\rm sw}$ is the O(a) improvement coefficient [22]. The constant c_M serves to optimize simulation algorithms and $c_0 = (1 + 8\kappa)^{-1}$. For all practical

simulations we have imposed an even/odd preconditioning and hence used the preconditioned matrix $\hat{Q}$, whose precise definition can be found in e.g. [23, 24]. It is the aim of the numerical simulations to compute expectation values of gauge invariant operators $\mathcal{O}$

$$\langle \mathcal{O} \rangle = \mathcal{Z}^{-1} \left[\int \mathcal{D}U e^{-S_g[U]} \det(Q^2[U]) \mathcal{O}[U] \right] , \tag{3}$$

using Monte Carlo methods. Note that in eq.(3) the square of the determinant appears in order to have a positive definite measure suitable for the numerical algorithms employed below.

In the PHMC algorithm a polynomial $P_{n,\epsilon}(Q^2)$, approximating $(Q^2)^{-1}$ for all eigenvalues λ of Q^2 with $\lambda \in [\epsilon, 1]$, is introduced such that $\det(P_{n,\epsilon}^{-1}(Q^2)) \approx \det(Q^2)$. Using the trivial identity $\det(Q^2) = \det(Q^2 P_{n,\epsilon}(Q^2))/\det(P_{n,\epsilon}(Q^2))$ and representing the determinants with the help of auxiliary bosonic fields ϕ and η, carrying colour and spin indices, one may exactly rewrite the partition function eq.(1) as

$$\begin{aligned} \mathcal{Z} &= \int \mathcal{D}U \mathcal{D}\phi^\dagger \mathcal{D}\phi \mathcal{D}\eta^\dagger \mathcal{D}\eta \, W \, e^{-(S_g + S_P + S_\eta)} \\ S_P &= S_P[U, \phi] = \phi^\dagger P_{n,\epsilon}(Q^2[U]) \phi \\ S_\eta &= \eta^\dagger \eta \, . \end{aligned} \tag{4}$$

In eq.(4) we have introduced the "correction factor" $W = W[\eta, U]$:

$$W = \exp\left\{ \eta^\dagger (1 - [Q^2 \cdot P_{n,\epsilon}(Q^2)]^{-1}) \eta \right\} . \tag{5}$$

Denoting averages evaluated with the effective action $S_g + S_P + S_\eta$ as $\langle \ldots \rangle_P$, the exact averages denoted as $\langle \ldots \rangle$ are obtained by reweighing with W

$$\langle \mathcal{O} \rangle = \langle W \rangle_P^{-1} \langle \mathcal{O} W \rangle_P \, . \tag{6}$$

As mentioned in the introduction, the advantage of rewriting the partition function in the form of eq.(4) is that by a suitable choice of the polynomial $P_{n,\epsilon}(Q^2)$ the eigenvalue spectrum of Q^2 can be smoothly separated into a part to be included in the update procedure by simulating the effective action $S_g + S_P$ and a rest, taken into account in the correction factor.

We remark that, in analogy to the case of the multiboson technique [25], the PHMC algorithm is also suited to allow for performing simulations with an odd

number of flavours. Of course, the above procedure leading to eq.(4) may be generalized and several polynomials may be introduced in such a way that each of them gives a good approximation in different parts of the eigenvalue spectrum. We demand in this case that the product of all these polynomials approximates the inverse of Q^2. The realization we are using in this paper amounts to cutting out the very low-lying end of the eigenvalue spectrum from the update step.
In principle, there is a great flexibility in choosing the polynomial to approximate Q^{-2}. In this work we follow ref.[7] and choose a Chebyshev approximation method to construct $P_{n,\epsilon}(Q^2)$. Since the polynomial we are going to use is detailed already in [7, 24] we will give here just its final form written in the product representation,

$$P_{n,\epsilon}(Q^2) = p_{n,\epsilon}(Q) = \prod_{k=1}^{2n} [\sqrt{c_k}(Q - r_k)] \ , \tag{7}$$

where the complex numbers r_k are given by

$$\begin{aligned} r_k &= \sqrt{z_k} = \mu_k + i\nu_k \ , \ \nu_k > 0 \ , \quad k = 1, \ldots, n \\ r_k &= r^*_{2n+1-k} \ , \quad k = n+1, \ldots, 2n \\ z_k &= \frac{1}{2}(1+\epsilon) - \frac{1}{2}(1+\epsilon)\cos(\frac{2\pi k}{n+1}) - i\sqrt{\epsilon}\sin(\frac{2\pi k}{n+1}) \ . \end{aligned} \tag{8}$$

The overall normalization constant, $\prod_{k=1}^{n} c_k$, can be computed analytically. If the c_k's are taken all identical, they turn out to be of O(1).
The polynomial $P_{n,\epsilon}(Q^2)$ approximates the inverse of Q^2 with a relative fit error which is bounded from above by

$$\delta \equiv 2\left(\frac{1-\sqrt{\epsilon}}{1+\sqrt{\epsilon}}\right)^{n+1} \ , \tag{9}$$

for all the eigenmodes of Q^2 with eigenvalues λ in the interval $\lambda \in [\epsilon, 1]$. The operator Q^2 is normalised (through the choice of c_M) in such a way that its largest eigenvalue is always smaller than 1. For eigenvalues $\lambda < \epsilon$ the relative fit error quickly increases as λ decreases.

2.2 Implementation and cost of the PHMC algorithm

The approximation of $\det(Q^2)$ through the inverse determinant of the polynomial $P_{n,\epsilon}(Q^2)$ was first suggested in [6]. There it led to a completely local bosonic action

involving n copies of bosonic fields. Since the bosonic action in that case was local, algorithms like heatbath and over-relaxation could be used. One unfortunate property of this approach was the observation that the autocorrelation time of the algorithm grows with the number of bosonic fields appearing in the action [9, 10].

The approximate fermion action S_P eq.(4) [5, 4] on the other hand still represents a non-local bosonic action. In this approach one therefore has to rely on small step size algorithms. However, the advantage is that now only one dynamical bosonic field is needed and hence the dangerous increase of the autocorrelation time with the number of bosonic field copies mentioned above is avoided.

In more detail, we have chosen to use a suitably adapted Φ-version [26] of the HMC algorithm for the update of the gauge fields. The usual arguments, including the reversibility of the molecular dynamics evolution, leading to the proof of detailed balance, still holds for the case of the PHMC algorithm. The implementation of this update method for the case of $\mathrm{O}(a)$ improved fermions and even/odd preconditioning can be done in complete analogy to ref. [23]. We therefore only want to point out some peculiarities which are not discussed in [23].

In the following discussion we will be somewhat sketchy and focus our attention on the modifications of the standard Φ-version of the HMC algorithm that are needed for implementing the PHMC algorithm. In particular, we note again that it is to be understood that for the actual simulation the preconditioned matrix $\hat{Q}$ was always used. Another remark is that the roots r_k, $k = 1, \ldots, 2n$ were suitably reordered with respect to their definition, eq.(8), while preserving the relation $r_{2n+1-k} = r_k^*$. Such a reordering is necessary to keep rounding errors on a tolerable level, as thoroughly discussed in [24]. Details of the different ordering schemes we have used in our implementation of the PHMC algorithm and rounding errors associated with them are discussed in Section 4.

In the PHMC algorithm the variation of the pseudofermion action, S_P eq.(4), with respect to a given gauge link is somewhat more complicated than in the standard HMC algorithm. In terms of the variation of the operator Q, denoted by δQ, it assumes the form

$$\delta S_P = \sum_{j=1}^{n} \left[\delta Q \; \chi_{j-1} \otimes \chi_{2n-j}^{\dagger} + \delta Q \; \chi_{2n-j} \otimes \chi_{j-1}^{\dagger} \right] \; , \tag{10}$$

where the auxiliary pseudofermion fields χ_j, for $j = 1, \ldots, 2n-1$ are defined as

$$\chi_j \equiv [\sqrt{c_j}(Q - r_j)] \cdot [\sqrt{c_{j-1}}(Q - r_{j-1})] \cdot \ldots \cdot [\sqrt{c_1}(Q - r_1)]\phi \qquad (11)$$

and ϕ denotes the pseudofermion field of eq.(4). In eq.(10) the products $\chi \otimes \chi^\dagger$ denote direct products in colour space and a trace over spin indices is understood. In order to speed up the simulation and minimize memory requirements we proceed for the computation of δS_P as follows: We first precalculate the n vectors χ_k, for all $k = 1, \ldots, n$ and store them. We then start the evaluation of the different contributions to δS_P by computing $\chi_{n-1} \otimes \chi_n^\dagger$ and its Hermitean conjugate, which for brevity will not be mentioned explicitly in the following. The next contribution to δS_P would involve $\chi_{n-2} \otimes \chi_{n+1}^\dagger$. The vector $\chi_{n+1}^\dagger$ is obtained by computing $(Q - r_{n+1})\chi_n$. The resulting vector can now be stored in χ_{n-1} since this vector is no longer used. Iterating this procedure results in a memory requirement of $n+1$ pseudofermion vectors. This may be considered as a drawback of the PHMC algorithm as it requires a substantial amount of memory if the degree of the polynomial becomes large. However, as it will be discussed below, there are several ways to overcome possible bottlenecks if not enough memory is available.

It is clear that the evaluation of all terms necessary to evaluate δS_P amounts to $(2n-1)$ $Q\phi$ operations (the extra work to incorporate the roots r_k in the operator $Q - r_k$ is completely negligible). In addition, since there are n terms to be summed (and traced) to evaluate eq.(10) and since each of them requires a computational work roughly equivalent (at least in our implementation on the APE computers) to one $Q\phi$ operation, the complete cost of the computation of δS_P will become about $3n$ $Q\phi$ operations.

Although the polynomial approximation to $(Q^2)^{-1}$ is rather precise even if a few eigenvalues of Q^2 occur that are slightly larger than one, the numerical construction of δS_P itself turns out to be unstable when eigenvalues very close to 1 are met in the updating procedure. At least in our implementation of δS_P, based on eq.(10), numerical overflows occurred when updating gauge configurations carrying modes of Q^2 with eigenvalues very close to (even if smaller than) 1. In practise, Q should therefore be normalized, through c_M in eq.(2), such that the average highest eigenvalue of Q^2 is sufficiently smaller than one, say $\langle \lambda_{\max} \rangle \approx 0.9$. Since the value of the highest eigenvalue of Q^2 shows very small fluctuations, such

an appropriate normalization can safely be done at the beginning of a simulation. The pseudofermion field ϕ in eq.(4) is to be generated according to the distribution $\exp\{-S_P[U,\phi]\}$. Generating this distribution via a heatbath step involves the computation of the inverse square root of $P_{n,\epsilon}(Q^2[U])$. This can be achieved by computing ϕ through

$$\phi = A^{\dagger}_{n,\epsilon}(Q)[Q^2 P_{n,\epsilon}(Q^2)]^{-1} Q^2 R_G \tag{12}$$

where R_G is a random Gaussian vector and $A_{n,\epsilon}$ is given by

$$A_{n,\epsilon}(Q) = \prod_{k=1}^{n} \sqrt{c_k}(Q - r_k) \; . \tag{13}$$

The vector $X = [Q^2 P_{n,\epsilon}(Q^2)]^{-1} Q^2 R_G$ is computed with a Conjugate Gradient (CG) method, solving the equation $Q^2 P_{n,\epsilon}(Q^2)\; X = Q^2 R_G$. We demanded that in generating ϕ with a CG inverter the relation

$$|S_P - R^{\dagger}_G R_G| \approx \mathrm{O}(10^{-7}) \tag{14}$$

holds. We noticed that this can be achieved by choosing a moderately large stopping criterion for the CG solver, namely $\epsilon_{\mathrm{stop}} = 10^{-12}$, where ϵ_{stop} is defined by the norm of the residual vector

$$\Phi_{\mathrm{res}} = Q^2 R_G - Q^2 P_{n,\epsilon}(Q^2)\; X \tag{15}$$

divided by the norm of the solution vector X (which is numerically close to the norm of $Q^2 P_{n,\epsilon}(Q^2)\; X$ in all practical cases):

$$\epsilon_{\mathrm{stop}} = \|\Phi_{\mathrm{res}}\|^2 / \|X\|^2. \tag{16}$$

A last remark concerns the second pseudofermion field η. It is generated trivially by Gaussian random vectors. Through it the correction factor $W = W[\eta, U]$ (eq.(5)) can be computed via the solution of the equation $[Q^2 P_{n,\epsilon}(Q^2)]X = \eta$, which involves an additional inversion of $Q^2 P_{n,\epsilon}(Q^2)$. The correction factor, or $w = \log(W)$ is then obtained by

$$w[\eta, U] = \eta^{\dagger}(1 - [Q^2 P_{n,\epsilon}(Q^2)]^{-1})\eta \; . \tag{17}$$

Since the expression $Q^2 P_{n,\epsilon}(Q^2)$ is almost the unit matrix, there is the possibility of dangerous rounding errors when computing the vector $(1 - [Q^2 P_{n,\epsilon}(Q^2)]^{-1})\eta$

in eq.(17), especially on machines with only 32-bit precision [1]. However, eq.(17) may be rewritten as

$$w[\eta, U] \equiv \eta^\dagger (R_{n,\epsilon}(Q^2)[Q^2 P_{n,\epsilon}(Q^2)]^{-1})\eta \ . \tag{18}$$

Following refs.[6, 7, 24] the polynomial $R_{n,\epsilon}(Q^2) = Q^2 P_{n,\epsilon}(Q^2) - 1$ is directly given by Chebyshev polynomials of degree $n+1$. One may hence use numerically stable recursion relations to compute $R_{n,\epsilon}(Q^2)$. Although the use of eq. (18), instead of eq. (17), leads to a somewhat larger cost for evaluating the correction factor, our experience is that it is advisable to use eq.(18) when only 32-bit precision is employed. Analogously to the case of generating the pseudofermion field ϕ, eq.(4), we optimized the value of the stopping criterion also for the CG inversion needed in eq.(18).

It might be observed[2] that eq.(17) can be generalized to

$$w[\eta, U] = \eta^\dagger (1 - [b_{n,\epsilon} Q^2 P_{n,\epsilon}(Q^2)]^{-1})\eta \ , \tag{19}$$

where $b_{n,\epsilon}$ is some real positive constant. Its value might be optimized, depending on the values of n and ϵ, in order to reduce the stochastic noise associated with reweighing through the correction factor. However, we did not exploit this additional freedom and took always $b_{n,\epsilon} = 1$, which enabled us to use the expression of $w[\eta, U]$ in eq.(18).

In principle, the ratio of the number of η-field "updates" to the number of gauge field updates is arbitrary. In fact, it turns out (see Section 3) that it is advantageous to choose this ratio to be larger than one. In this way, the additional noise induced in the reweighted observables, eq.(6), by the correction factor can be partly suppressed. The above-mentioned ratio will be denoted in the following by $N_{\rm corr}$, since it gives the number of computations of the correction factor per gauge field configuration.

From the discussion above it is easy to express the cost of the PHMC algorithm in terms of matrix times vector, $Q\phi$, operations. The cost for the PHMC algorithm can be split into three parts,

$$C_{Q\phi}(PHMC) = C_{\rm bhb} + C_{\rm update} + C_{\rm corr} \ , \tag{20}$$

[1] We remark that, of course, all internal products and global sums were performed in software Kahan or double precision arithmetic.

[2] We are grateful to Ulli Wolff for this interesting remark.

where $C_{\rm bhb}$ is the cost for the heatbath of the bosonic fields, $C_{\rm update}$ the cost for the computation of δS_P and $C_{\rm corr}$ the cost to evaluate the correction factor. In units of $Q\phi$ operations we find

$$\begin{aligned} C_{\rm bhb} &= (2n+2)\cdot N_{\rm CG}^{\rm bhb} + n \\ C_{\rm update} &= 3n \cdot N_{\rm step} \\ C_{\rm corr} &= (2n+2)\cdot N_{\rm CG}^{\rm corr} \cdot N_{\rm corr} \ . \end{aligned} \tag{21}$$

The factor $N_{\rm corr}$ denotes as above the number of evaluations of the correction factor W per full gauge field update (or molecular dynamics trajectory). The symbols $N_{\rm CG}^{\rm bhb}$ and $N_{\rm CG}^{\rm corr}$ denote the average numbers of CG iterations in the heatbath of the bosonic fields and the computation of W, respectively. The factor $3n$ in $C_{\rm update}$ comes from adding the cost for the construction of the auxiliary fields χ_k and the cost of the other algebraic operations needed for a single update of the gauge field and its conjugate momenta. $N_{\rm step}$ is the number of steps used in a trajectory, i.e. how often δS_P has to be evaluated within a trajectory. We explicitly verified that our formulae for $C_{\rm update}$, $C_{\rm bhb}$ and $C_{\rm corr}$ agree with the costs in real time observed for our implementation of the PHMC algorithm on the APE computer.

The scaling behaviour of the computational cost $C_{\rm update}$, eq.(21), as a function of the lattice size, $L^3 \times T$, or the condition number of Q^2 is expected to be fully analogous to the one observed in the HMC algorithm, with one important difference. Due to the form of the variation of the pseudofermion action, S_P eq.(4), in the molecular dynamics evolution for the PHMC algorithm the role of the lowest eigenvalue of Q^2 is taken over by the infrared cut–off parameter of the polynomial approximation, ϵ, as already discussed in [4]. Since in practise $\epsilon \approx 2\langle\lambda_{\rm min}\rangle$, we expect therefore an improvement on the cost of a simulation.

3 Effects of the correction factor

In this section we want to discuss the effects of the correction factor we introduced for the exactness of the algorithm. The first main point concerns the statistical fluctuations induced by reweighing observables with the correction factor: this aspect determines to a large extent the tuning of the PHMC algorithm. The

second point is of qualitative nature and concerns the occurrence of gauge configurations with exceptional eigenvalues of Q^2 and how the reweighing procedure can deal with them.

3.1 Statistical errors and reweighing

As discussed above, an important ingredient of the PHMC algorithm is the correction factor. The computational cost of the algorithm will depend in a crucial way on the behaviour of the correction factor in a real simulation. The reason is that through the correction factor, which is computed stochastically, a certain noise is introduced which may affect the errors on the observables and will contribute therefore to the cost of a simulation.
In the PHMC algorithm the update of the gauge field U is alternated with $N_{\rm corr}$ "updates" of the pseudofermion field η, yielding $N_{\rm corr}$ evaluations of $W[\eta, U]$ on each gauge configuration. Performing a simple arithmetic average of them yields a single estimate of the correction factor per each gauge configuration. As a consequence, on a sample of N gauge configurations labelled by the integer j, the averages $\langle \ldots \rangle_P$ introduced in section 2.1 can be represented as trivial arithmetic averages over the sample:

$$\langle \mathcal{O}W \rangle_P = N^{-1} \sum_{j=1}^{N} \mathcal{O}_j W_j \tag{22}$$

where $\mathcal{O}_j$ is any gauge invariant observable and W_j the above alluded estimate of the correction factor on the gauge configuration U_j.
For any finite number of configurations, the statistical error on $\langle \mathcal{O} \rangle$ is expected to depend on the choice of n and ϵ, i.e on the chosen polynomial approximation to $(Q^2)^{-1}$, and, for a given polynomial approximation, also on the value of $N_{\rm corr}$. By rewriting the expression for the reweighted average of $\mathcal{O}$, eq.(6), in the form:

$$\langle \mathcal{O} \rangle = \langle \mathcal{O} \rangle_P + \langle W \rangle_P^{-1} \cdot (\langle \mathcal{O}W \rangle_P - \langle \mathcal{O} \rangle_P \langle W \rangle_P) \ , \tag{23}$$

it becomes clear that both the statistical fluctuations of $\mathcal{O}$ and those of the connected part of $\mathcal{O}W$ contribute to the statistical error on the reweighted average, eq.(23). The latter contribution will depend on the statistical correlation between the observable $\mathcal{O}$ and the reweighing factor W.

As the polynomial approximation to $(Q^2)^{-1}$ is made more precise, the contribution to the error on $\mathcal{O}$ coming from the statistical correlation between $\mathcal{O}$ and W becomes smaller, just because W gets closer to 1. Still, in the limit $W \approx 1$, there remains some noise, because W is computed not exactly but only stochastically. We are then left with a pure Gaussian noise factor.

Choosing a poor polynomial approximation to $(Q^2)^{-1}$ for the update step in the PHMC algorithm yields a reweighing factor W which will strongly fluctuate. (Think, e.g., of W as being the full determinant.) Moreover, W may have in general a non-negligible correlation with the observable $\mathcal{O}$, such that, even in the limit $N_{\rm corr} \to \infty$, a large contribution to the error on $\langle \mathcal{O} \rangle$ is expected to arise. The discussion suggests that it is the relative statistical error of the correction factor itself that controls the additional fluctuations induced by reweighing and hence the statistical error for a given observable $\langle \mathcal{O} \rangle$.

As a consequence, we can expect the PHMC algorithm to be found efficient only in situations where the variance of W is very small. This amounts to choosing the value of ϵ to be of the same order as the average lowest eigenvalue of (Q^2) and the value of n to be large enough for the polynomial approximation to $(Q^2)^{-1}$ to be reasonably precise. As we will see below, situations of this kind can be realized, in practice, by setting $\epsilon \approx 2\langle \lambda_{\rm min} \rangle$ and n such that the fit accuracy $\delta \approx 0.01$, see eq.(9). When this criterion is respected and hence the parameters of the polynomial are fixed, the statistical error on $\langle \mathcal{O} \rangle$ will only be a function of $N_{\rm corr}$. In the following we will see which values of $N_{\rm corr}$ are sufficient to keep the error on $\langle \mathcal{O} \rangle$ small.

A most important quantity in determining the cost of a simulation of a given algorithm is the autocorrelation time. Since we are using the correction factor to render the algorithm exact, all observables have to be computed as a ratio of $\langle \mathcal{O} W \rangle_P$ and $\langle W \rangle_P$: hence it is not obvious how to define the autocorrelation function of $\mathcal{O}$, in terms of which the integrated autocorrelation time $\tau_{\rm int}(\mathcal{O})$ is usually defined. We "define" the integrated autocorrelation time for a given observable $\mathcal{O}$ by means of the expression which can be derived in the ordinary case, when no reweighing occurs:

$$\tau_{\rm int}(\mathcal{O}) = \frac{1}{2} \left(\frac{\sigma(\mathcal{O})}{\sigma^{\rm naive}(\mathcal{O})} \right)^2 \tag{24}$$

where $\sigma^{\rm naive}(\mathcal{O})$ denotes the naive and $\sigma(\mathcal{O})$ the true error on the observable $\mathcal{O}$. In order to obtain a reliable estimate of the true error on $\mathcal{O}$ in all of our tests, which are discussed below, we have used a single elimination jack-knife procedure. The jack-knife procedure has been then combined with a binning analysis by blocking the data into blocks of length $L_{\rm block}$. Our error analysis follows closely the discussion in [18] (see section 5.2 there).

We have run K replica in parallel and determined the true error in two ways: In the first approach we average on each replicum separately. Since the averaged data are statistically independent, we can estimate the true error by looking at the naive dispersion of them with respect to their arithmetic average. The *relative* error on the error in this case can be estimated as $(2K)^{-1/2}$. In the second approach, we divide the sample into blocks of size $L_{\rm block}$, so that the total number of blocks is given by $N_{\rm block} = KN_{\rm traj}/L_{\rm block}$, where $N_{\rm traj}$ is the number of trajectories obtained per replicum. Of course, $L_{\rm block}$ is to be constrained by the requirement that data coming from different replica never appear in the same block. The error can then be computed as a function of the block length $L_{\rm block}$. For a large enough block length, a plateau behaviour sets in from which we then determine the true error. The *relative* error on the error in this procedure can be estimated as $(2N_{\rm block})^{-1/2}$.

Even when we have determined the true error on an observable as discussed above, the definition of the naive error on $\langle\mathcal{O}\rangle$, and consequently the autocorrelation time $\tau_{\rm int}(\mathcal{O})$, is not obvious, again due to the occurrence of the reweighing factor W in the definition of $\langle\mathcal{O}\rangle$. A possible definition of the naive error on $\langle\mathcal{O}\rangle$ is given by the single elimination jack-knife error for a block length of $L_{\rm block} = 1$. We remark however that the variance of $\mathcal{O}$:

$$\mathcal{V}(\mathcal{O}) = \langle\mathcal{O}^2\rangle - \langle\mathcal{O}\rangle^2 = \frac{\langle\mathcal{O}^2 W\rangle_P}{\langle W\rangle_P} - \frac{\langle\mathcal{O}W\rangle_P^2}{\langle W\rangle_P^2} \tag{25}$$

is an observable itself and should hence be independent of a particular algorithm used to compute it. The above observation suggests another definition of the naive error on $\langle\mathcal{O}\rangle$, which is the one adopted in our studies of the PHMC algorithm:

$$\sigma^{\rm naive}(\mathcal{O}) = \Big[(N-1)^{-1}\mathcal{V}(\mathcal{O})\Big]^{1/2} \ . \tag{26}$$

with $N = KN_{\rm traj}$. Note that only for $W = 1$ both definitions of the naive error have to agree.

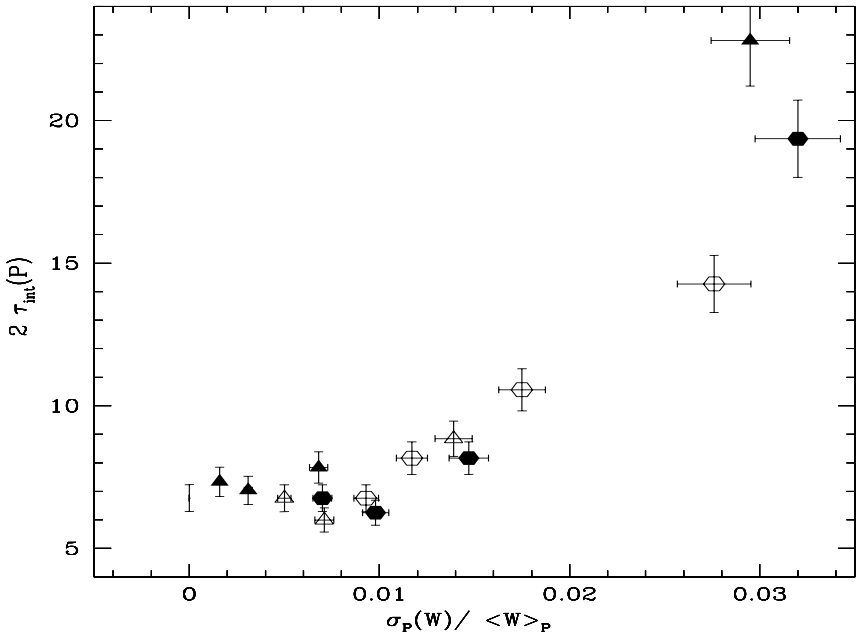

Figure 1: The integrated autocorrelation time for the plaquette, $2\tau_{\rm int}(P)$, versus $\sigma_P(W)/\langle W\rangle_P$, for several values of ϵ: $\epsilon = 0.046$ (empty hexagones), $\epsilon = 0.036$ (filled hexagones), $\epsilon = 0.026$ (empty triangles), $\epsilon = 0.016$ (filled triangles). For each value of ϵ four values of n (8, 12, 16, 20) are considered: the smaller is n, the larger is the corresponding value of $\sigma_P(W)/\langle W\rangle_P$ in the plot.

3.2 Tuning of the PHMC algorithm

In order to investigate on a quantitative level the tuning problem for n, ϵ and $N_{\rm corr}$, we have run the PHMC algorithm on a 4^4 lattice with Schrödinger functional boundary conditions [20, 21] for a number of choices of n and ϵ. To be more specific, we have set $c_t(g_0) = 1$ and $\theta = \pi/5$. At the boundary at time $t = 0$ the gauge fields were set to classical fields denoted as point "A" in [20]. Finally, the gauge fields at time $t = T$ were set to be identical to the one at $t = 0$. We remark that since we have chosen the gauge fields to be identical at both time boundaries, we do *not* have exactly the same boundary conditions as the ones in [20]. The simulation parameters were chosen to be $c_{\rm sw} = 0$, $\beta = 6.4$ and $\kappa = 0.15$. Although in this situation the average condition number for $\hat{Q}^2$ was only about 60 we still

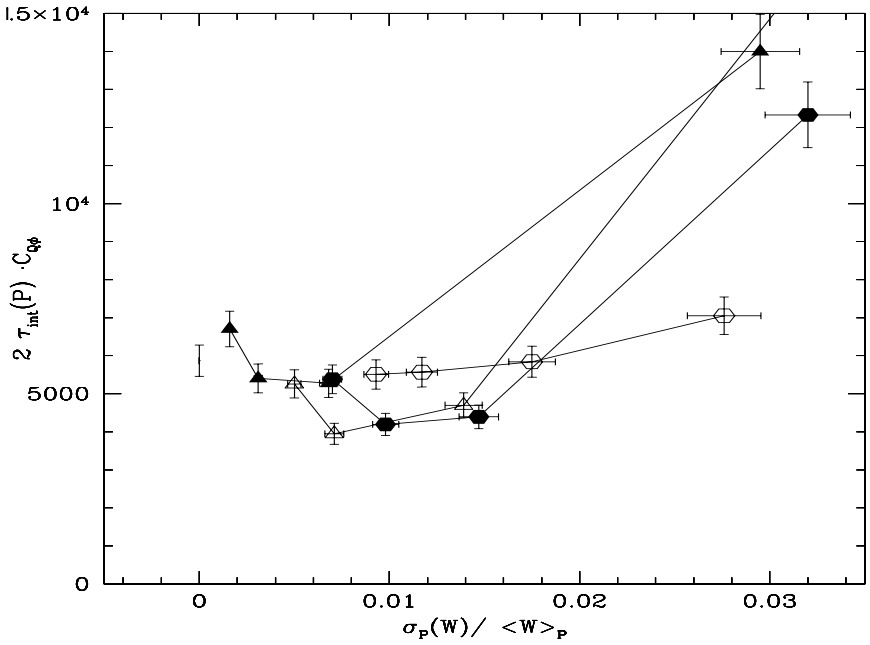

Figure 2: The cost of obtaining a statistically independent measurement of the plaquette, $2\tau_{\rm int}(P)\cdot C_{Q\phi}$ is plotted versus $\sigma_P(W)/\langle W\rangle_P$, using the same symbols as in Fig.1.

find a significant dependence of the simulation cost on the algorithm parameters such that a sensible tuning can be performed. For each choice of n and ϵ about 20000 trajectories were generated using a step size of $\delta\tau = 0.25$ and the number of molecular dynamics steps $N_{\rm md} = 4$. These parameters were chosen to yield acceptance rates of about 80%. The values of $N_{\rm corr}$ were varied from 1 to 4 or 1 to 10 in these simulations. These values for $N_{\rm corr}$ turned out to be sufficient to look for an optimal value minimizing the computational cost. We will consider here mainly two observables, the plaquette and the lowest eigenvalue of $\hat{Q}^2$, denoted by P and $\lambda_{\rm min}$, respectively. We mention that we monitored also the largest eigenvalue of $\hat{Q}^2$ and the reweighing factor itself. Within statistical errors the average values for all the considered observables agree among all our simulations with the PHMC algorithm and with the corresponding results obtained from the HMC algorithm.

We start by showing the integrated autocorrelation time of the plaquette observ-

able in Fig. 1. As discussed above we expect the cost of a simulation using the PHMC algorithm to depend strongly on the relative fluctuation of the correction factor. We therefore plot the integrated autocorrelation time as a function of $\sigma_P(W)/\langle W\rangle_P$. Here the subscript P (not to be confused with the symbol for the plaquette) reminds that the mean value and the standard deviation for the correction factor W do not involve, of course, any reweighing and

$$\sigma_P(W) = \left[(N_{block}-1)^{-1}(\langle W^2\rangle_P - \langle W\rangle_P^2)\right]^{1/2} \ . \tag{27}$$

For the figure we have chosen four values of ϵ (0.046, 0.036, 0.026, 0.016) and n (8, 12, 16, 20). The smaller n is, the larger is the corresponding value of $\sigma_P(W)/\langle W\rangle_P$ in the plot. For each choice of n and ϵ, we took the value of $N_{\rm corr}$ that turns out to minimize the quantity $2\tau_{int}(P)C_{Q\Phi}$ (see below). The point at $\sigma_P(W)/\langle W\rangle_P = 0$ belongs to the integrated autocorrelation time as obtained from the HMC algorithm. It is clearly seen that when increasing $\sigma_P(W)/\langle W\rangle_P$ the integrated autocorrelation time assumes large value. For $\sigma_P(W)/\langle W\rangle_P < 0.01$, the dependence of the autocorrelation time becomes weak and no preferred choice of n and ϵ can be given.

In Fig. 2 we show the total cost by computing $2\tau_{\rm int}(P)C_{Q\Phi}$, with the cost factor $C_{Q\Phi}$ given in eq.(20), again taking for each n and ϵ the value of $N_{\rm corr}$ that minimizes $2\tau_{\rm int}(P)C_{Q\Phi}$ itself. Here we find that for $\sigma_P(W)/\langle W\rangle_P \approx 0.01$ one reaches the minimal cost of the algorithm. We also give, at $\sigma_P(W)/\langle W\rangle_P = 0$, the cost of a corresponding HMC simulation. As already mentioned in [4] the cost obtained from the PHMC algorithm is significantly lower. On the other hand, for $\sigma_P(W)/\langle W\rangle_P > 0.01$ the cost from the PHMC algorithm increases, which is a direct consequence of the increase of the autocorrelation time observed in Fig. 1. For $\sigma_P(W)/\langle W\rangle_P \ll 0.01$ we also find an increase of the cost of the simulation. This is a consequence of the fact that more precise polynomial approximations have a higher computational cost without giving any sensible reduction of the autocorrelation time $\tau_{\rm int}(P)$ and, correspondingly, of the statistical error $\sigma(P)$. The corresponding results for $\lambda_{\rm min}$ look qualitatively similar, although with a somewhat stronger dependence on $\sigma_P(W)/\langle W\rangle_P$. Also in this case we find the optimal value of $\sigma_P(W)/\langle W\rangle_P \approx 0.01$.

After having identified the optimal values for n and ϵ, it is interesting to study the behaviour of the statistical errors as a function of the values of $N_{\rm corr}$. To this end,

$L^3 \times T$	Algor.($N_{\rm corr}$)	$< P >$	$< \lambda_{\rm min}(\hat{Q}^2) >$
4^4	HMC	0.66179(5)[12]	0.01582(3)[8]
4^4	PHMC(4)	0.66186(5)[12]	0.01582(3)[8]
	PHMC(3)	0.66185(5)[12]	0.01583(3)[8]
	PHMC(2)	0.66185(5)[12]	0.01583(3)[8]
$\rightarrow$	PHMC(1)	0.66185(5)[12]	0.01583(3)[8]
	PHMC(0)	0.66221(5)[12]	0.01451(3)[8]
4^4	PHMC(10)	0.66188(5)[18]	0.01588(3)[16]
	PHMC(9)	0.66188(5)[18]	0.01584(3)[16]
	PHMC(7)	0.66198(5)[19]	0.01586(3)[17]
	PHMC(5)	0.66198(5)[20]	0.01581(3)[17]
$\rightarrow$	PHMC(4)	0.66201(5)[22]	0.01584(03)[18]
	PHMC(3)	0.66213(5)[23]	0.01575(3)[19]
	PHMC(2)	0.66215(5)[28]	0.01569(3)[22]
	PHMC(1)	0.66218(5)[36]	0.01553(3)[24]
	PHMC(0)	0.66272(5)[16]	0.01218(3)[8]

Table 1: The behaviour of mean values and statistical errors for the plaquette and the lowest eigenvalue of $\hat{Q}^2$ as a function of $N_{\rm corr}$: data are obtained with the HMC and the PHMC algorithms. For the latter we have considered the parameters $n = 8$, $\epsilon = 0.036$ (data set with $N_{\rm corr}$ ranging from 1 to 10) and $n = 16$, (data set with $N_{\rm corr}$ ranging from 1 to 4). The statistics has been 21000 trajectories in all cases. We give in round brackets the naive error and in square brackets our estimate for the true error. An arrow points towards the line where the value of $N_{\rm corr}$ turns out to be basically optimal. The case $N_{\rm corr} = 0$ in the PHMC data refers to the results obtained with no reweighing.

we have chosen two different values of n and ϵ. The first one, $n = 16$ and $\epsilon = 0.026$ corresponds to $\sigma_P(W)/\langle W \rangle_P \approx 0.01$ and is therefore considered to be close to the optimal value. The other choice is $n = 8$ and $\epsilon = 0.036$, which gives a value of $\sigma_P(W)/\langle W \rangle_P \simeq 0.032$ and is clearly far from being optimal. The mean values for the plaquette P and eigenvalue $\lambda_{\rm min}$ as well as the naive (round bracket) and true (square bracket) errors are given in table 1. The value of $N_{\rm corr} = 0$ corresponds to the case where no reweighing is performed, which is expected to

yield systematically wrong results. For the non-optimal choice of n and ϵ we observe a strong dependence of the statistical errors on $N_{\rm corr}$. The lowest values of σ are obtained only for $N_{\rm corr} = 10$, i.e. the largest of the considered values of $N_{\rm corr}$. Even the values of σ corresponding to $N_{\rm corr} = 10$ are still somewhat larger (especially for $\lambda_{\rm min}$) than both the statistical errors for $N_{\rm corr} = 0$ and from the HMC algorithm. This behaviour closely corresponds to what is expected from the above discussion about the statistical noise induced by the reweighing procedure. On the other hand, when considering the optimal choice of n and ϵ, the statistical errors from the PHMC algorithm do not show any visible dependence on $N_{\rm corr}$ and basically coincide with the ones from the HMC algorithm. Finally we remark that in all cases the mean values are consistent among themselves within the measured statistical errors. Moreover, the naive errors, defined according to eq.(26), are also consistent among all cases considered here.

The behaviour of the error on the plaquette and $\lambda_{\rm min}$ was also tested on an 8^4 lattice for parameter values $\beta = 5.6$, $\kappa = 0.1585 \simeq \kappa_c$, $c_{\rm sw} = 0$. The Schrödinger functional boundary conditions that we adopted were chosen to be the same as for the 4^4 lattice mentioned above. The only difference is that the boundary improvement coefficient was set to its 1-loop value, i.e. $c_t(g_0) = 1.0 - 0.089 g_0^2$. The statistics in this case is 2700 trajectories. We refer to [4] for a more detailed information about the algorithmic parameters and give our results in table 2. We compare the results obtained using the PHMC algorithm (in the setup with $K = 32$ replica) with the ones obtained using the HMC algorithm. We performed also a control run for the PHMC algorithm on only 1 replicum running up to the same statistics of 2700 trajectories. This gave completely consistent results, as it should, of course, and provided us with a further check of our estimate of the uncertainty on the true error given in braces in table 2. From table 2 we infer that in this case the practically optimal value of $N_{\rm corr}$ appears to be 2 or 3 and is hence again reasonably small when a good polynomial approximation is chosen. The results on the 8^4 lattice were obtained by taking $n = 48$ and $\epsilon = 0.0026$, yielding a relative fit error $\delta \simeq 0.013$. This value of δ is even slightly larger than the relative fit error corresponding to the optimal choice of n and ϵ on the lattice 4^4, when the condition number of Q^2 was about 10 times smaller. This seems to indicate that, even if the statistical fluctuations of the correction factor are expected to increase with the lattice volume and the condition number

$L^3 \times T$	Algor.($N_{\rm corr}$)	$< P >$	$< \lambda_{\rm min}(\hat{Q}^2) >$
8^4	HMC	0.57251(04)[12]{3}	0.001310(10)[51]{8}
8^4	PHMC(4)	0.57253(5)[14]{3}	0.001318(10)[50]{8}
	PHMC(3)	0.57248(5)[14]{3}	0.001318(10)[50]{8}
$\rightarrow$	PHMC(2)	0.57249(5)[15]{3}	0.001328(10)[50]{8}
	PHMC(1)	0.57260(5)[19]{5}	0.001310(10)[60]{10}
	PHMC(0)	0.57272(5)[12]{2}	0.001141(10)[45]{7}

Table 2: The behaviour of mean values and statistical errors for the plaquette and the lowest eigenvalue of $\hat{Q}^2$ as a function of $N_{\rm corr}$ on a 8^4 lattice. The notation is the same as in table 1. The numbers in braces give our estimate of the uncertainty on the true error.

of Q^2, it might be unnecessary to take polynomial approximations more and more severe. This might be explained by the observation that in this case also autocorrelation times generally increase, leading to a larger number of evaluations of the correction factor on statistically correlated gauge configurations; in some cases, moreover, the statistical fluctuations of physical observables increase, too. However we think that further and much more time-consuming studies are needed to clarify the issue.

3.3 Exceptional eigenvalues

So far, we have discussed the PHMC algorithm for situations where no exceptional eigenvalues of Q^2, i.e. those that are orders of magnitude smaller than the average lowest eigenvalue, appear. However, the PHMC algorithm is designed to allow especially for the occurrence of gauge field configurations carrying exceptionally small eigenvalues of Q^2. In fact we expect the probability of generating such configurations with the PHMC algorithm to be considerably larger than the corresponding probability when using the HMC algorithm or exact versions of the multiboson technique with accept/reject step.

This expectation is indeed confirmed in a real simulation, as can be seen from Fig. 3. There we plot the distribution of the lowest eigenvalue of $\hat{Q}^2$ as obtained from simulations with the HMC and the PHMC algorithms. The parameters for

the runs were chosen to be $\beta = 5.4$, $\kappa = 0.1379$ and $c_{\rm sw} = 1.7275$. The lattice size was $8^3 \times 16$ and Schrödinger functional boundary conditions were adopted as specified in [18].

Clearly, the distribution obtained from the PHMC algorithm stretches to much smaller values of λ. However, after reweighing with the correction factor, the average lowest eigenvalue obtained in this case from the PHMC algorithm takes a value consistent with the one obtained from the HMC algorithm. In Fig. 4 we show the (Monte Carlo) time evolution of the 10 lowest eigenvalues. We find that there is a band of eigenvalues at a level roughly corresponding to the average lowest eigenvalue and that only occasionally an *isolated* eigenvalue gets very small[3]. This is exactly the situation anticipated in ref. [4]. As also discussed there, if $\lambda_{\rm min} \ll 1$, when computing the correction factor exactly on each gauge configuration, i.e. taking $N_{\rm corr} = \infty$, $W = \det[Q^2 P_{n,\epsilon}(Q^2)]$ turns out to be proportional to $\lambda_{\rm min}$. Hence the correction factor serves the purpose of cancelling divergences in certain quark Green functions. In the following discussion we neglect the distinction between the operator Q^2, which is certainly the relevant one for quark Green functions, and some preconditioned form of it, which may be conveniently used in the update and reweighing procedures. Indeed, doing so does not affect our conclusions and keeps the discussion more general.

In practise the evaluation of the correction factor on gauge configurations carrying exceptionally small eigenvalues may be problematic, since the badly conditioned operator $Q^2 P_{n,\epsilon}(Q^2)$ has to be inverted and $N_{\rm corr}$ is usually taken to be a finite (relatively small) number.

We see from eq.(18) that the quantity $[Q^2 P_{n,\epsilon}(Q^2)]^{-1}\eta$ is needed for the evaluation of the reweighing factor as described above. The inversion of $Q^2 P_{n,\epsilon}(Q^2)$ is performed by using a CG algorithm, where suitable vectors are multiplied by $Q^2 P_{n,\epsilon}(Q^2)$ several times. As discussed in [24], the multiplication of $Q^2 P_{n,\epsilon}(Q^2)$ is affected by rounding-error effects, which can be kept on a tolerable level in normal situations. However, on gauge configurations carrying exceptionally small eigenvalues of Q^2, these rounding-error effects might be significantly amplified, especially for the components of $[Q^2 P_{n,\epsilon}(Q^2)]^{-1}\eta$ having non-vanishing projection on the low lying mode eigenvectors.

[3] In some rare cases we have observed that the same happens for two or three eigenvalues.

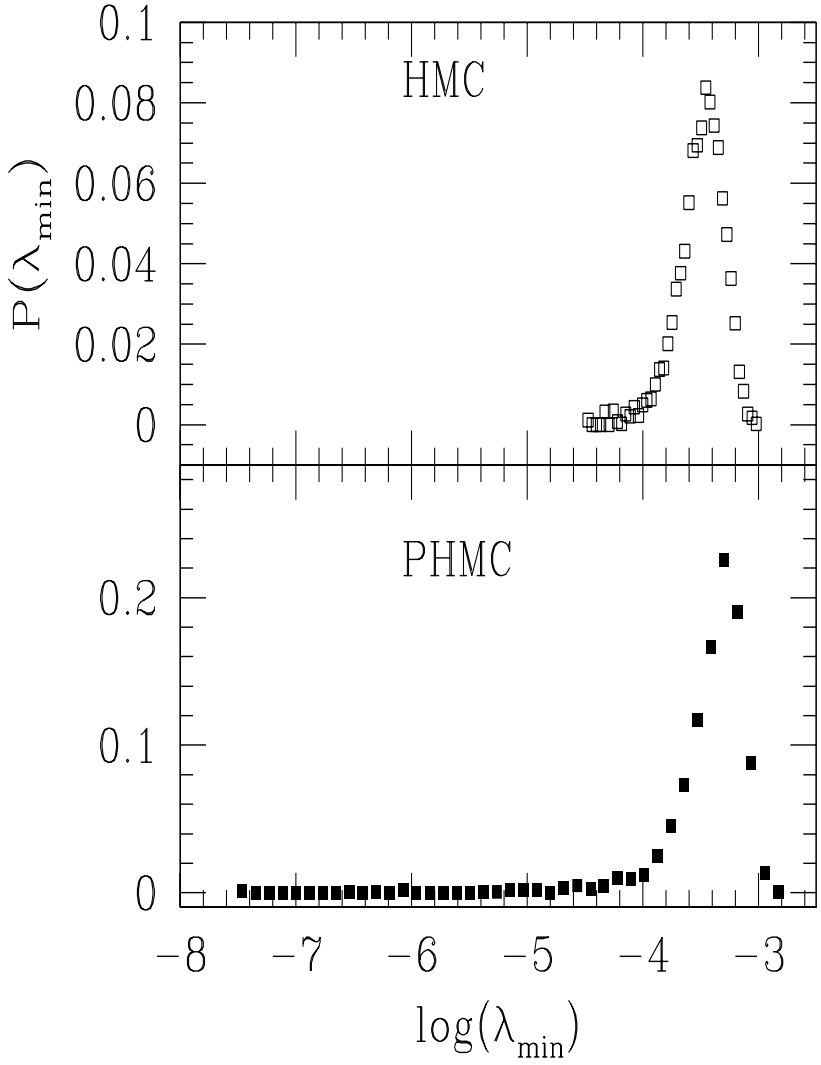

Figure 3: The distributions of the lowest eigenvalue $\lambda_{\min}$ of $\hat{Q}^2$ as obtained from the HMC and the PHMC algorithms. The quantity $P(\lambda_{\min})$ denotes the number of eigenvalues for a given bin, normalized by the total number of eigenvalues. Both runs have the same statistics.

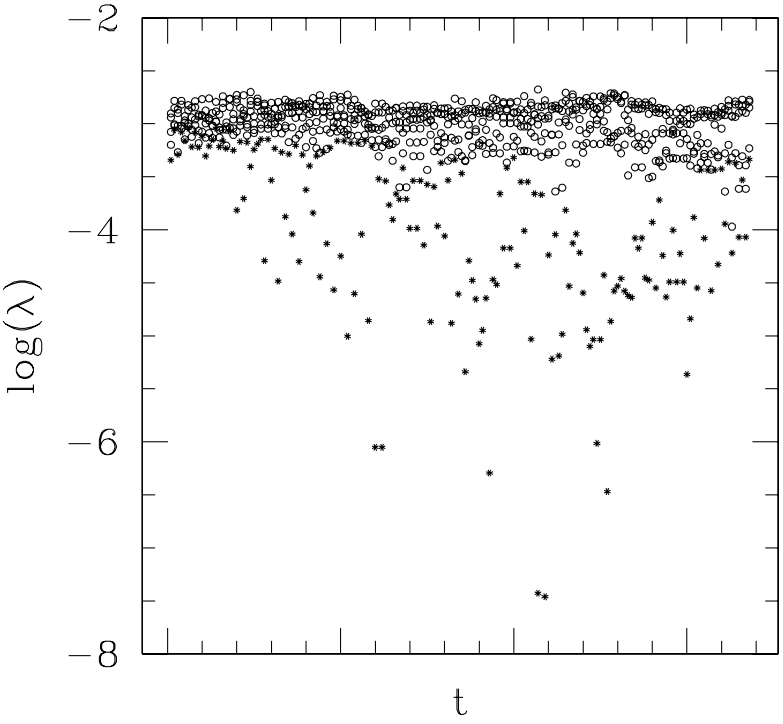

Figure 4: The Monte Carlo time evolution of the five lowest eigenvalues from a simulation using the PHMC algorithm. We denote by the stars the lowest eigenvalue and for the open circles the remaining ones.

In order to see the potential problems arising from taking a finite value of $N_{\rm corr}$, let us introduce the eigenvalues λ_j and eigenvectors $|\lambda_j\rangle$ of Q^2,

$$Q^2|\lambda_j\rangle = \lambda_j|\lambda_j\rangle \ . \tag{28}$$

Then the correction factor $W = \exp(w[\eta, U])$ of eq.(18) becomes

$$w[\eta, U] \ = \ \sum_j |\langle\lambda_j|\eta\rangle|^2 R_{n,\epsilon}(\lambda_j)(1 + R_{n,\epsilon}(\lambda_j))^{-1} \ . \tag{29}$$

Since $R_{n,\epsilon}(\lambda) \to -1$ as $\lambda \to 0$, all random fields η that have a sizeable projection on the low–lying modes of Q^2 yield very large negative values of w and hence exponentially small values of W are obtained. The dominant contributions to the correction factor will come when the projection of the fields η on the exceptional modes is almost zero. In practise the correction factor is evaluated stochastically by setting $N_{\rm corr}$ to a small value and taking for the correction factor on a given gauge configuration U the following noisy estimate:

$$W[U; N_{\rm corr}] = N_{\rm corr}^{-1} \sum_{j=1}^{N_{\rm corr}} W[\eta_j, U] \ . \tag{30}$$

It is, of course, very unlikely that a field η with almost vanishing projection on the zero mode will be generated. As a consequence, the noisy estimate of the reweighing factor obtained on a gauge configuration carrying low–lying modes of Q^2 is likely to be very imprecise. On the other hand, an exact evaluation of the reweighing factor of eq.(30) with $N_{\rm corr} = \infty$ will give that $W \propto \lambda_{\rm min}$ as desired. The above discussion makes it clear that the computation of the correction factor, as explained above for "normal" situations, should be generalized to deal with the case where exceptional eigenvalues occur. To this end we introduce another infrared cut-off parameter $\tilde{\epsilon} \ll \epsilon$ and write the partition function as

$$\begin{aligned} \mathcal{Z} \ &= \ \int \mathcal{D}U\mathcal{D}\phi^\dagger\mathcal{D}\phi\mathcal{D}\eta^\dagger\mathcal{D}\eta \ W_B W_{IR} \ e^{-(S_g+S_P+S_\eta)} \\ S_P \ &= \ S_P[U,\phi] = \phi^\dagger P_{n,\epsilon}(Q^2[U])\phi \\ S_\eta \ &= \ \eta^\dagger\eta \end{aligned} \tag{31}$$

where now the original correction factor W is split into two parts, an "infrared" part,

$$W_{IR} = \prod_{\lambda_j \le \tilde{\epsilon}} [1 + R_{n,\epsilon}(\lambda_j)] \tag{32}$$

and a "bulk" part

$$W_B[\eta, U] = \exp\left\{\eta_\perp^\dagger [R_{n,\epsilon} \cdot (Q^2 \cdot P_{n,\epsilon})^{-1}]\eta_\perp\right\} \ , \tag{33}$$

where

$$|\eta_\perp\rangle = |\eta\rangle - \sum_j \theta(\tilde{\epsilon} - \lambda_j)|\lambda_j\rangle\langle\lambda_j|\eta\rangle \ . \tag{34}$$

The infrared part of the correction factor W_{IR} is very much in the spirit of ref.[7], where also the underlying assumption was taken that only a few isolated small eigenvalues occur. Exact observables are now computed through

$$\langle\mathcal{O}\rangle = \langle W_B W_{IR}\rangle_P^{-1} \langle\mathcal{O} W_B W_{IR}\rangle_P \ . \tag{35}$$

In order to guarantee the exactness of the simulation algorithm, $\tilde{\epsilon}$ has to be *fixed* in a given simulation. We give in appendix A a derivation of eq.(33) which explicitly shows how the splitting of the original correction factor W into W_B and W_{IR} is fully determined *a priori* by the choice of $\tilde{\epsilon}$. Of course, when no eigenvalues smaller than $\tilde{\epsilon}$ occur, $W_{IR} = 1$ and it has not to be computed. In the case that such eigenvalues occur, the two correction factors W_B and W_{IR} can be computed by evaluating all eigenvalues $\lambda_j \leq \tilde{\epsilon}$ and the corresponding eigenvectors.

Obviously, W_B in eq.(33) receives no contribution from the low-lying modes ($\lambda_j \leq \tilde{\epsilon}$) of Q^2. This property of W_B justifies the expectation that a noisy reweighing with W_B in eq.(35) can be performed by choosing a small, finite value for the number of η-field "updates" N_B. From this point of view, the statistical noise induced by reweighing with W_B is expected to be quantitatively very similar to the one induced in "normal" situations by the reweighing factor W, eq.(5) and the values for N_B should in practise be similar to the values usually chosen for $N_{\rm corr}$.

We have tested the modified correction factor in practise by taking a gauge configuration carrying a mode of Q^2 with an exceptionally low eigenvalue (about $3 \cdot 10^6$ times smaller than the highest one). Indeed, the estimate of $\det[Q^2 P_{n,\epsilon}(Q^2)]$ obtained from the original reweighing factor W is very imprecise and converges very slowly to the correct value when increasing $N_{\rm corr}$. As a consequence one finds a large variance of W as a function of η. On the other hand, the improved estimate of $W[U]$ given by $W_{IR}[U]W_B[U; N_B]$, where

$$W_B[U; N_B] = N_B^{-1} \sum_{j=1}^{N_B} W_B[\eta_j, U] \tag{36}$$

and $\tilde{\epsilon} = \epsilon/10$, is much less noisy already for pretty small values of N_B. In fact, the fluctuations are fully analogous to the case when no exceptional eigenvalues are present. More quantitative information on this point will be given in a forthcoming publication [19].

We remark that the problem of inverting the operator $Q^2 P_{n,\epsilon}(Q^2)$ in the subspace orthogonal to the one spanned by the low–lying modes of Q^2 is always well conditioned, even in the presence of an exact zero mode. The evaluation of $\eta_\perp$ can be done by computing all the eigenvectors of Q^2 corresponding to eigenvalues smaller than $\tilde{\epsilon}$. Since, as shown in Fig.1, there are usually only a few isolated eigenvalues below $\tilde{\epsilon}$, these eigenvalues and the corresponding eigenvectors can be calculated reliably by using the techniques described in [29].

The level of precision needed in computing the low-lying eigenvalues and the corresponding eigenvectors of Q^2 is determined by requiring that the uncertainties in W_{IR} and W_B, induced by the uncertainties on these eigenvalues and eigenvectors, be negligible (with respect to the statistical fluctuations of W_{IR} and W_B). Using the fact that $R_{n,\epsilon}(\lambda) \simeq -1 + c\lambda$, with $c = O(\epsilon^{-1})$, the relative uncertainty on each factor in the product of eq.(32) can be estimated (for $\lambda \ll 1$) as

$$[1 + R_{n,\epsilon}(\lambda)]^{-1} \delta [1 + R_{n,\epsilon}(\lambda)] \simeq \lambda^{-1} \delta\lambda \; , \tag{37}$$

where $\delta\lambda$ denotes the uncertainty on a given eigenvalue λ. On the other hand, the uncertainties in the determination of the eigenvectors corresponding to eigenvalues smaller than $\tilde{\epsilon}$ directly affect the evaluation of $|\eta_\perp\rangle$, eq.(34), and hence W_B, eq.(33).

The discussion above makes very straightforward the software implementation of the proposed reweighing procedure: once a value for $\tilde{\epsilon}$ has been set, the program has just to check on each generated gauge configuration whether the lowest eigenvalue of Q^2 is smaller than $\tilde{\epsilon}$. Only in the affirmative case, of course, does the correction factor $W_B W_{IR}$ actually differ from the usual one and an evaluation of W_{IR} is required.

It might be observed that, if the PHMC update ever generates gauge configurations with a *significant* fraction of the modes of Q^2 belonging to very low eigenvalues, the above described reweighing procedure becomes computationally very expensive. This is certainly true, but in that case troubles are also expected in the evaluation of quark propagators by ordinary CG–like inverters. Indeed, it is likely

that in such a situation a relatively precise knowledge of all the low–lying modes is needed even for evaluating the fermion Green functions. This can be done by splitting each quark propagator into two parts: the first part, to which only the low-lying modes contribute, should be expressed in terms of the known eigenvalues and eigenvectors; the second part, to which no low-lying modes contribute, should be evaluated by inverting the operator Q in the subspace orthogonal to the one spanned by the low–lying modes of Q^2.

4 Rounding errors in the PHMC algorithm

Rounding errors may become in principle a problem for all simulation algorithms. Each algorithm is designed to produce field configurations according to a probability distribution, related to the Boltzmann factor of a given Euclidean field theory. The danger is that when implementing a code for some finite precision computer, rounding errors may render the probability distribution of the actually produced field configurations somewhat different from the desired one. In particular, when using molecular dynamics kind of algorithms like the HMC or the PHMC algorithms, the equations of motion, integrated numerically by a symplectic integrator, lack in principle the reversibility condition, resulting in an inexact algorithm. It is still an open question for what situations this systematic error of the molecular dynamics kinds of algorithm will become important in practise.

The problem of rounding errors ought to be studied especially for the PHMC algorithm. As the discussion in section 2.2 showed, for an efficient computation of δS_P in the PHMC algorithm, the product representation of the polynomial $P_{n,\epsilon}$ should be used. However, the stability of the numerical construction of the polynomial in the product representation depends strongly on the ordering of the monomial factors in eq. (7). Particularly "bad" orderings easily lead to substantial precision losses or even numerical overflow. As demonstrated in [24] (see also [30]), there exist, fortunately, orderings of the monomial factors (or equivalently the roots of the polynomial) such that rounding errors can be kept on a perfectly tolerable level.

Still, the rounding errors appearing for a particular ordering scheme applied in a given situation should be monitored carefully. In the generation of the pseudo-

fermion fields ϕ one could in principle resort to numerically stable recursion relations. However, as discussed above, it is very easy to monitor the rounding errors in this case by evaluating the difference of eq.(14). In the evaluation of the correction factor, on the other hand, it is in general advisable to use a recursion relation [27, 28] in order to obtain a sufficiently precise result. In the following we will first discuss the rounding-error effects appearing in the construction of $Q^2 P_{n,\epsilon}(Q^2)$: this is the polynomial of highest degree among the ones which occur in the PHMC update and all the different polynomials of lower degree are numerically constructed by using the same ordering of monomial factors. We then turn to a discussion of the magnitude of reversibility violations.

4.1 Rounding errors from the product representation

As shown in [24], the Clenshaw recursion relation provides a very stable and precise way to evaluate the polynomial $Q^2 P_{n,\epsilon}(Q^2) = 1 + R_{n,\epsilon}(Q^2)$, even when 32 bit precision is employed everywhere, but in internal products and other sums over the whole lattice. This gives us the possibility of evaluating the size of the rounding errors when the polynomial $Q^2 P_{n,\epsilon}(Q^2)$ is constructed in its product representation, eq. (7). Following [24] we consider the vector

$$\Phi_{\mathrm{order}} \equiv \hat{Q}\sqrt{c_n}(\hat{Q} - r_n) \cdot \ldots \cdot \sqrt{c_1}(\hat{Q} - r_1)\hat{Q} R_G \tag{38}$$

where we have taken the preconditioned matrix $\hat{Q}$ as it was used in all our numerical tests. The label "order" can stand for a particular monomial ordering scheme. In the following we will only discuss the bit reversal and Montvay's schemes, which were found in [24] to be the most precise. We refer again to [24] for a definition of the ordering schemes employed here. Given the numerical stability of the Clenshaw recursion, a good measure of rounding errors, when only 32 bit precision is employed, is the quantity

$$\Delta_{\mathrm{order}} = \frac{1}{\sqrt{N}} \| \Phi_{\mathrm{order}} - \Phi_{\mathrm{Clenshaw}} \| \ . \tag{39}$$

In table 3 we give the results for Δ_{order} for the bit reversal and Montvay's ordering schemes. All results have been obtained on an $8^3 \times 16$ lattice with Schrödinger functional boundary conditions as used for the computation for the O(a) improved

Table 3: The quantity $\Delta_{\rm order}$ eq. (39) is given for the bit reversal (BR) and Montvay's ordering schemes.

n	ϵ	δ	$\Delta_{\rm BR}$	$\Delta_{\rm Montvay}$
16	0.0030	0.310	$3.1(1)10^{-6}$	$3.0(1)\cdot 10^{-6}$
32	0.0030	0.054	$3.3(1)10^{-6}$	$3.0(1)\cdot 10^{-6}$
64	0.0022	0.0045	$4.5(1)10^{-6}$	$4.2(1)\cdot 10^{-6}$
100	0.0022	0.0002	$8.4(2)10^{-6}$	$6.4(2)\cdot 10^{-6}$
100	0.0010	0.0034	$9.0(2)10^{-6}$	$6.4(2)\cdot 10^{-6}$
100	0.0005	0.0218	$10.8(2)10^{-6}$	$7.8(2)\cdot 10^{-6}$

action [18]. The parameters of the runs were $\beta = 6.8$, $\kappa = 0.1343$ and $c_{\rm sw} = 1.42511$.

We have chosen the constants c_k, eq.(7), to be all identical. Choosing the c_k's different from each other (while keeping fixed their product which guarantees the proper normalization of $P_{n,\epsilon}$), changes the results in table 3 at most at the 10% level. The results of table 3 are qualitatively very similar to the ones reported in [24]. They show a growth of rounding errors in the construction of the polynomial $P_{n,\epsilon}$ as n and ϵ^{-1} increase (see the behaviour for $n = 100$). However, the magnitude of rounding errors for the cases considered in table 3 are perfectly tolerable. In particular, no evidence for numerical instabilities or large rounding error effects has been observed. Since all our simulations are performed using either the bit reversal or Montvay's ordering schemes for a range of values of n and ϵ covered by the ones given in table 3, we conclude that our numerical simulations are safe against rounding errors coming from the use of the product representation for the polynomial $P_{n,\epsilon}$.

4.2 Reversibility violations

For the purposes of this section, the evolution of the gauge field in the molecular dynamics part of the PHMC algorithm can be summarized as follows: some initial field configuration of the gauge fields $U_{x,\mu}$ and their conjugate momenta $\pi_{x,\mu}$, $\{U_{\rm in}, \pi_{\rm in}\}$, is evolved from a fictitious Monte Carlo time $t = 0$ to the final

configuration $\{U_{\rm end}, \pi_{\rm end}\}$ at $t = T$, with T usually set to $T = 1$ in production runs. This evolution is determined by the "equations of motion", derived from a Hamiltonian $H = \frac{1}{2}\sum_{x,\mu} \pi^2_{x,\mu} + S$, where S is the total action. At $t = T$, the configuration $\{U_{\rm end}, \pi_{\rm end}\}$ is subject to an accept/reject step using the values of the Hamiltonians $H_{\rm in}$ and $H_{\rm end}$, as measured on the initial and final configurations, respectively.

We recall that in evolving the gauge field configuration in the Monte Carlo time a great flexibility is allowed. The imposed restrictions are –from a practical point of view– that the acceptance rate determined by $H_{\rm end} - H_{\rm in}$ should be reasonably large, about 80%, and –from a principal point of view– that the evolution in the Monte Carlo time ought to be reversible in order to guarantee detailed balance and consequently the correct importance sampling.

The method of choice for the Monte Carlo time evolution is to evolve the system with the equations of motion using a leap-frog integrator. It was found, in particular when machines with only 32-bit precision arithmetic are used, that due to rounding errors, violations of the reversibility condition are encountered. What is worse, it appears that the equations of motion correspond to those of a classical chaotic system with a positive Liapunov exponent [31, 32, 33, 34, 35]. As a consequence, rounding error effects are exponentially amplified along the integration of the equations of motion.

Using a leap-frog integrator –in particular on an APE machine with 32-bit arithmetic as in this work– needs therefore an estimate of violations of reversibility. As it was discussed at length in [24], in the PHMC algorithm some orderings of the monomial factors in the product representation can lead to large rounding-errors effects with a possible strong influence on reversibility violations. We therefore checked the magnitude of the reversibility violations when using the subpolynomial, the bit reversal and Montvay's ordering schemes as described in [24]. These tests were performed with the same parameters as in Section 4.1. In particular, the polynomial parameters were chosen to be $n = 64$ and $\epsilon = 0.0022$.

To measure the reversibility violations, we simply started from the final configuration $\{U_{\rm end}, \pi_{\rm end}\}$, reversed the sign of the step size dt and integrated back to reach the reversed configuration $\{U_{\rm rev}, \pi_{\rm rev}\}$. In all our tests we used the higher order leap-frog integrator as suggested in [36] (i.e. eq.(6.7) of that reference with $n = 4$). Our step size was chosen to be $dt = 0.05$ for both the forward and the

backward integration and the value of the trajectory length was $T = 0.75$. On the initial and the reversed configurations we measured the corresponding Hamiltonians $H_{\rm in}$ and $H_{\rm rev}$ and the plaquettes $P_{\rm in}$ and $P_{\rm rev}$ averaged over the gauge configuration. The difference of these quantities, dH, dP and the norm difference dU of the gauge links

$$\begin{aligned} \|dU\|^2 &= \|U_{\rm in} - U_{\rm rev}\|^2 = \frac{1}{36V} \sum_{x,\mu,\alpha,\beta} |U_{\rm in}^{x,\mu,\alpha,\beta} - U_{\rm rev}^{x,\mu,\alpha,\beta}|^2 \\ dH &= |H_{\rm in} - H_{\rm rev}| \\ dP &= |P_{\rm in} - P_{\rm rev}| \end{aligned} \tag{40}$$

serve as our quantitative measure of the reversibility violations. In eq.(40) the sum extends over the lattice points, the 4 forward directions and the colour indices.

Table 4: Reversibility violations for the PHMC and HMC algorithms, comparing different root orderings for the PHMC algorithm, subpolynomial (SP), bit reversal (BR) and Montvay's ordering scheme. BR* indicates that the roots are calculated in 64-bit arithmetic.

Scheme	$\langle \|dU\| \rangle$	$\langle dH \rangle$
SP	$9.45(1) \cdot 10^{-6}$	$2.1(2) \cdot 10^{-2}$
BR	$1.293(1) \cdot 10^{-6}$	$4.0(9) \cdot 10^{-3}$
BR*	$1.292(1) \cdot 10^{-6}$	$2.8(8) \cdot 10^{-3}$
Montvay	$1.277(1) \cdot 10^{-6}$	$3.4(9) \cdot 10^{-3}$
HMC	$6.7(2) \cdot 10^{-7}$	$1.4(6) \cdot 10^{-3}$

Our results, averaged over 32 configurations are given in table 4 for the subpolynomial (SP), the bit reversal (BR) and Montvay's ordering scheme. We compare with the corresponding results from the HMC algorithm, using there the same number of steps and an equal step size as used in the case of the PHMC algorithm. For the HMC algorithm, in the Conjugate Gradient solver we have chosen a stopping criterion requiring that the squared norm of the residual vector, normalized by the solution vector, be less than $\epsilon_{\rm stop}^{\rm HMC} = 10^{-14}$.
One clearly sees that the subpolynomial scheme gives substantially more reversibility violations than the one encountered in the HMC algorithm. Within

the errors, the size of the reversibility violations from the PHMC algorithm with the bit reversal and Montvay's scheme are of the same order as the ones from the HMC algorithm. We also considered the bit reversal ordering in the case, denoted as BR*, when the roots and the normalization factors are computed with 64-bit precision and then read in. Within the errors we do not find any effect. In our tests we could find no difference in the plaquette expectation value. We conclude that our results are not contaminated from reversibility violation effects.

As mentioned above, there is a lot of flexibility to perform the evolution of the gauge field configuration in Monte Carlo time in the molecular dynamics part of the HMC algorithm. The PHMC algorithm establishes an approximation of the exact evolution. The crucial advantage of the PHMC algorithm is, of course, that this approximation is fully controlled and can be corrected for. Another possibility of approximating the Monte Carlo time evolution is to just use a larger stopping criterion for the inverter of $\hat{Q}^2$. However, we think that the reversibility violations, which are certainly present, may then become dangerous: due to rounding errors, when integrating the gauge fields backward in time, the inverter "sees" a different gauge field configuration from the one during the forward integration. Therefore also the solution vectors will be different and when the stopping criterion is relaxed, this difference is enhanced, possibly leading to large reversibility violations.

This effect is amplified when one makes use of the "knowledge of the past": the inverter is started with an initial guess, which is the solution of the previous inversion. This reduces the number of iterations in the inverter, since generally the movement of the gauge fields through configuration space is smooth. The idea may also be iterated [33]. However, in this way potential rounding errors are amplified, since they are accumulated in the solution vectors.

A possible solution may be to choose always a constant starting vector. Then reversibility violations only appear through the difference in the gauge field configuration. We tested this possibility for our implementation of the HMC algorithm and report our results in table 5. A similar investigation has been performed in [34]. Here we have taken the same parameters as used for table 4, averaging again over 32 configurations.

As can be seen, already for a stopping criterion of 10^{-10} the reversibility violations are substantially larger than for the severe stopping criterion, showing even a

Table 5: Comparison of reversibility violations in the HMC algorithm using a constant starting vector in the Conjugate Gradient solver.

$\epsilon_{\text{stop}}^{\text{HMC}}$	$\langle \|\|dU\|\| \rangle$	$\langle dH \rangle$	$\langle dP \rangle$
$1.0 \cdot 10^{-14}$	$6.58(1) \cdot 10^{-7}$	$1.1(6) \cdot 10^{-3}$	$--$
$1.0 \cdot 10^{-12}$	$8.5(1) \cdot 10^{-7}$	$1.8(7) \cdot 10^{-3}$	$--$
$1.0 \cdot 10^{-10}$	$2.6(4) \cdot 10^{-6}$	$7.8(1.8) \cdot 10^{-3}$	$6(3) \cdot 10^{-8}$
$1.0 \cdot 10^{-8}$	$4.7(3) \cdot 10^{-5}$	$2.0(3) \cdot 10^{-1}$	$6(1) \cdot 10^{-7}$

difference in the expectation value of the plaquette. We conclude that on machines with 32-bit precision arithmetic the stopping criterion can not be relaxed too much. Since with a constant starting vector we loose the advantage of having a reasonable first guess for the solution of the inverter, we prefer using a severe stopping criterion and a better initial guess over relaxing the stopping criterion and using a constant starting vector. Of course, the situation might look different on machines with higher precision, where reversibility violations are suppressed. We would like to point out a second effect relevant for reversibility violations. When the stopping criterion is made large, it might happen that during the backward integration the inverter stops one iteration before or later than on the corresponding step in the forward integration. Since now the stopping criterion is large, the solution vectors are very different, leading to large reversibility violations. The only way to overcome this would be to also keep the number of iterations constant. However, we feel that with this way of accelerating the algorithm the convergence of the inverter is not very well controlled, but we have not studied this situation in detail and we do not know how a possible poor convergence may affect the acceptance of the whole molecular dynamics trajectory.

5 Memory requirements

In this section we wish to discuss three possible ways of reducing memory requirements. The first two ways (sections 5.1 and 5.2) result in some reasonably tolerable computational overhead. The last way (section 5.3) was already shortly mentioned in [4] but it leads to a significant alteration of the dynamics.

Once again, we neglect in our discussion the technical complications arising from the use of even–odd preconditioning, which can however be treated as in any HMC–like algorithm. We recall here that the pseudofermion fields ϕ and $\chi_k, \quad k = 1, 2, \ldots$, which will enter our discussion, are assigned to arrays defined on all lattice sites. Indeed, even if only the odd–site components are needed in principle, we have found it convenient to make use of the even–site components to store intermediate results in the construction of the operator $\hat{Q}$ (see eq.(35) of [24]), which connects second neighbour sites on the original lattice.

5.1 PHMC update with $(Q^2 - z_k)$ monomials

It is, of course, possible to implement the PHMC algorithm by using also the product representation

$$P_{n,\epsilon}(Q^2) = \prod_{k=1}^{n} [c_k(Q^2 - z_k)] \tag{41}$$

with the roots z_k given in eq.(8). The variation of the action S_P then becomes

$$\delta S_P = \sum_{k=1}^{n/2} c_k \left[\delta Q^2 \; \xi_{k-1} \otimes \xi^{\dagger}_{n-k} + \delta Q^2 \; \xi_{n-k} \otimes \xi^{\dagger}_{k-1} \right] \; , \tag{42}$$

where the auxiliary pseudofermion fields ξ_k, for $k = 1, \ldots, n-1$ are given by

$$\xi_k \equiv [c_k(Q^2 - z_k)] \cdot [c_{k-1}(Q^2 - z_{k-1})] \cdot \ldots \cdot [c_1(Q^2 - z_1)]\phi \; . \tag{43}$$

Following the discussion in section 2.2, the evaluation of δS_P in eq. (42) implies a memory requirement of only $(n/2) + 2$ pseudofermion fields, which means a reduction of basically a factor 2.

However, if one insists on using only $(n/2) + 2$ pseudofermion fields, it seems impossible to avoid an overhead on the computational cost. In evaluating δS_P in eq.(42) one needs, analogously to the case discussed in Section 2.2, $3n$ $Q\phi$ operations. There appear, however, additional $n/2$ $Q\phi$ operations for the following reason. When storing only the fields $\xi_1, \ldots, \xi_{n/2}$ before starting the computation of δS_P, one is "loosing" the information about the vectors $Q\xi_1, \ldots, Q\xi_{n/2-1}$, which have already been calculated as intermediate steps in the evaluation of the auxiliary fields $\xi_1, \ldots, \xi_{n/2}$. This information is needed since $\delta Q^2 = [\delta Q]\, Q + Q\, [\delta Q]$. A similar problem with the vectors $Q\xi_l$ for $l = n/2, \ldots, n-1$ can be avoided by a

prudent usage of memory space associated with the vectors ξ_l. As a consequence, with respect to the method described in Section 2.2, when using the product representation of eq.(41), the memory requirements are basically halved at the price of an increase of the computational cost of δS_P, which can be estimated to be about 15–20%.

5.2 Flexible trading between memory requirement and CPU time

It is clear that in implementing the evaluation of δS_P, eq.(10), one can trade off CPU time with memory space in different ways. We sketch here the basic idea of a flexible method for compromising between memory and CPU time, which we have found very convenient in practical simulations. For simplicity we take the example of a polynomial, $P_{n,\epsilon}(Q^2)$, eq.(7), with $n = 100$ and consider a non-optimized version of the method that we use in practice. A fully general and very detailed technical discussion of this method and its performance is deferred to Appendix B.

A significant fraction of the memory is usually taken to store the gauge links, their conjugate momenta, some pseudofermion vectors, as needed for the fermion matrix inversion, and the dynamical pseudofermion field, ϕ, extracted from a probability distribution $\propto \exp\left[-\phi^\dagger P_{n,\epsilon}(Q^2)\phi\right]$. Let us imagine to divide the remaining storage space (assumed to be much less than what is needed for storing $n = 100$ pseudofermion vectors) into three sectors. In this particular case, with $n = 100$, the first and the second sector will contain 9 and the third sector only 2 pseudofermion vectors. It is clear that the third sector can be used as working space for fermion matrix times vector multiplications, where neither the initial vector nor the final one need to be stored elsewhere.

We have already observed in Section 2.2 that the variation δS_P, eq.(10), of the pseudofermion action S_P, is a sum of n terms. Each term depends only on two auxiliary fields, χ_{j-1}, χ_{2n-j} (and their complex conjugates), where j is the index over which the sum runs and the auxiliary vectors χ_k are defined in eq.(11). For the evaluation of δS_P one can then proceed as follows.

In a preliminary step, starting from ϕ, we construct the auxiliary vectors χ_1, χ_2, $\ldots$, χ_{89}, χ_{90}, and store *only* 9 vectors, namely χ_{10}, χ_{20}, $\ldots$, χ_{80}, χ_{90}, in the part

of the memory that we have indicated above as the first sector.
Then, in a first step, starting from the saved vector χ_{90}, we construct the auxiliary vectors χ_{91}, χ_{92}, ..., χ_{98}, χ_{99} and store all of them in the second sector. We are now in position to evaluate the first ten contributions to δS_P, namely the ones corresponding to $j = 100, 99, \ldots, 91$ in eq.(10). The point is that fermion matrix times vector multiplications can be performed in such a way that the third sector is employed to store *in turn* first χ_{100} and χ_{101}, then χ_{101} and χ_{102}, and so on, up to χ_{108} and χ_{109}.
In the second step, starting from the saved vector χ_{80}, we construct the auxiliary vectors χ_{81}, χ_{82}, ..., χ_{88}, χ_{89} and store all of them in the second sector. We are now in position to evaluate further ten contributions to δS_P, namely the ones corresponding to $j = 90, 89, \ldots, 81$ in eq.(10), making use of the third sector to temporarily store the various pairs of auxiliary vectors between χ_{110} and χ_{119}, as explained above.
Proceeding in an analogous way, we can evaluate in ten steps all the contributions to δS_P. Notice that in each of these steps, except the first one, nine pseudofermion vectors, which had been computed and immediately overwritten during the preliminary step mentioned above, are computed again. This leads to a global computational cost, which is equivalent to about 390 $Q\phi$ operations, to be compared with the cost of about 300 $Q\phi$ operations needed for the method discussed in section 2.2 (for a single evaluation of δS_P). This increase of the computational cost is just the price to be paid for evaluating δS_P in the case $n = 100$ by using only 20 (instead of 100) auxiliary pseudofermion vectors. A similar result, with somewhat better compromise between memory and CPU time, is found for any value of the degree n of the PHMC polynomial when using the generalized version of this method which is described in Appendix B.
Let us conclude with a general remark about the well-known problem of large memory requirements, which is in principle common to all algorithms for dynamical fermions relying on a polynomial approximation of some negative power of the Dirac operator. The method presented in this section clearly shows that this problem, even for a polynomial of very high degree n, is in practice much less severe for the PHMC algorithm than for the multiboson algorithm. This is a consequence of the fact that the number of dynamical pseudofermion fields is n in the multiboson algorithm and only one in the PHMC. This allows in the latter

case for a balance between the conflicting requirements of minimizing the number of auxiliary pseudofermion fields and maximizing the computational efficiency.

5.3 Introducing more pseudofermion fields

The last method of reducing memory requirements that we have studied amounts to introducing more pseudofermion fields and distributing the monomial factors of the polynomial $P_{n,\epsilon}(Q^2)$ among them. Let us consider the action

$$S_P^{(m)} = S_P^{(m)}[\phi, U] = \sum_{i=1}^{m} \phi_i^\dagger p_{n,\epsilon;m}^{(i)}(Q)\phi_i \ . \tag{44}$$

In eq.(44) we have introduced m positive definite subpolynomials $p_{n,\epsilon;m}^{(i)}(Q)$ each of degree $2n/m$ such that their product yields $P_{n,\epsilon}(Q^2)$. In this way, one has to have memory space for only $m + n/m$ pseudofermion fields in practise and hence would significantly reduce the memory requirements.
However, it is clear already at this stage that by changing m the dynamics of the algorithm will change: for $m = 1$ we recover our PHMC algorithm. For $m = n$ we are in the case of the original multiboson algorithm and would have an increase of the autocorrelation time with n. It might be hoped, however, that by choosing m small enough, the dynamics is not changed too much and that in this way again a reduction of memory requirements can be achieved.
It should be emphasized that when using the action eq.(44) special care has to be taken for the ordering of the roots in order not to generate unwanted effects that come purely from rounding errors. Without going into detail here, we note that by using e.g. the bit-reversal scheme, a suitable ordering of the roots avoiding rounding-error effects can be obtained. In addition, we checked that by running the program with 64-bit precision our results, quoted below, did not change.
We have done several tests for different choices of m in the range $m \in [2, 10]$. We report our results obtained in the $SU(2)$ gauge theory with two flavours of dynamical Wilson fermions. We set $c_{\rm sw} = 0$ and take a lattice of size $8^3 \times 16$ with periodic boundary conditions. We have considered two choices of the bare parameters, $\beta = 2.12$, $\kappa = 0.15$ and $\beta = 1.75$, $\kappa = 0.165$, using the subpolynomial and the bit-reversal ordering schemes of monomial factors.
The effects for different choices of m should most clearly appear in the Hamilto-

nian

$$H = \frac{1}{2}\sum_{x,\mu}\sum_{c=1}^{3}(\pi_\mu^c(x))^2 + S_g[U] + S_P^{(m)}[\phi, U]\ , \tag{45}$$

used in the molecular dynamics part of the PHMC algorithm. In eq.(45) π_μ denote the momenta conjugate to the gauge fields. We monitored the differences between the initial and final Hamiltonians in a molecular dynamics trajectory. For all parameters considered in table 6 we always started from the same thermalized gauge field configuration and kept the step size $dt = 0.04$ and the number of steps $N_{\rm step} = 10$ fixed.

In table 6 we give our results for the differences of the initial and final Hamiltonians $H_{\rm end} - H_{\rm in}$, of the gauge links $\|U_{\rm end} - U_{\rm in}\|$ and of their conjugate momenta ($\|\pi_{\rm end} - \pi_{\rm in}\|$), as measured at the beginning and at the end of a trajectory. The definition of $\|U_{\rm end} - U_{\rm in}\|^2$ is analogous to the definition of $\|U_{\rm in} - U_{\rm rev}\|^2$, eq.(40), with a normalisation factor of $(16V)^{-1}$ because the gauge group is now $SU(2)$. Finally, we define

$$\|\pi_{\rm end} - \pi_{\rm in}\|^2 = \frac{1}{12V}\sum_{x,\mu,c}|(\pi_\mu^c(x))_{\rm end} - (\pi_\mu^c(x))_{\rm in}|^2\ . \tag{46}$$

Table 6: The differences of the initial and final values of the Hamiltonian, the momenta and the gauge links. Results are obtained on a $8^3 \times 16$ lattice at $\beta = 1.75$, $\kappa = 0.165$, in the $SU(2)$ gauge theory.

n	ϵ	(m, order)	$H_{\rm end} - H_{\rm in}$	$\|\pi_{\rm end} - \pi_{\rm in}\|^2$	$\|U_{\rm end} - U_{\rm in}\|^2$
64	0.0015	(1, BR)	0.63	0.301	0.0657
64	0.0015	(1, SP)	0.63	0.301	0.0657
64	0.0015	(8, BR)	28.1	1.170	0.0357
64	0.0015	(8, SP)	40.9	1.158	0.0354
64	0.0005	(1, BR)	1.33	0.310	0.0655
64	0.0005	(8, BR)	101	0.856	0.0222

As the results shown in table 6 indicate, the behaviour of the molecular dynamics part of the algorithm looks such that in the case with $m = 8$ one typically gets *larger* time discretisation effects. This is clearly seen by the values of $H_{\rm end} - H_{\rm in}$. At the same time, the difference in the momenta $\|\pi_{\rm end} - \pi_{\rm in}\|$ becomes larger,

too, while the difference in the gauge links $\|U_{\rm end} - U_{\rm in}\|$ becomes *smaller* than in the case $m = 1$. This might be explained by the fact that the gauge links are always normalized to SU(2) matrices and that they counteract the behaviour of the momenta to render the difference $H_{\rm end} - H_{\rm in}$ small. The results depend also on the distribution of the monomial factors among the subpolynomials $p^{(i)}_{n,\epsilon;m}$, eq.(44), as the comparison between the bit-reversal and the subpolynomial cases shows. When reducing the value of ϵ we again find even more different results, as shown by the last two lines of table 6. Tests performed with gauge group SU(3) and Schrödinger functional boundary conditions revealed a similar qualitative behaviour.

We conclude that, in order to get a reasonable acceptance rate in the cases with $m > 1$, one is forced to reduce the value of dt substantially, resulting in a higher cost of a simulation. It seems to us that the case $m = 1$, i.e. the PHMC algorithm is most efficient. Of course, we cannot exclude that there are other possibilities of choosing subpolynomials that give a reduction of memory requirements and do not worsen the dynamical behaviour of the algorithm. On the other hand, the solution to the problem of memory requirement discussed in section 5.2 appears to be already satisfactory.

6 Conclusions

We gave in this paper a detailed description of the PHMC algorithm, which relies on a combination of the HMC algorithm and the multiboson technique to simulate dynamical fermions [5, 4]. We discussed the computational cost of the algorithm, checked that rounding-error effects that can appear are under control and showed possible ways to reduce memory requirements.

The effects of the correction factor that is introduced to render the algorithm exact, was studied in detail. Special emphasis was put on the fact that the PHMC algorithm samples the configuration space very differently compared to the most commonly used HMC algorithm. In particular, some evidence was given that the region of gauge configuration space characterized by the presence of low lying modes of Q^2 is explored much better when using the PHMC algorithm.

Of course, it is important to compare the performance of the PHMC algorithm

with the one of the HMC algorithm. The work presented here lays the ground for such an investigation of the performance of the PHMC algorithm on which we will report in a separate publication [19]. There we will also show further evidence that the PHMC algorithm samples configuration space differently from the HMC algorithm and discuss consequences for physical observables.

Acknowledgements

This work is part of the ALPHA collaboration research programme. We are most grateful to S. Aoki, B. Bunk, R. Sommer, P.Weisz and U. Wolff for many useful discussions and helpful comments. In particular we thank U. Wolff for a critical reading of the manuscript and M. Lüscher for essential advices and discussions. We thank DESY for allocating computer time to this project. R.F. thanks the Alexander von Humboldt Foundation for the financial support for his research stay at DESY–Hamburg, where part of this work was done.

A Derivation of eq.(33)

We start again from the $n_f = 2$ lattice QCD partition function, eq.(31):

$$\begin{aligned} \mathcal{Z} &= \int \mathcal{D}U\mathcal{D}\phi^\dagger\mathcal{D}\phi\mathcal{D}\eta^\dagger\mathcal{D}\eta\, W_B[\eta,U]W_{IR}[U]\; e^{-(S_g+S_P+S_\eta)} \\ S_P &= S_P[U,\phi] = \phi^\dagger P_{n,\epsilon}(Q^2[U])\phi \\ S_\eta &= \eta^\dagger\eta\;. \end{aligned} \tag{47}$$

The splitting of the original correction factor W into two parts, an "infrared" part,

$$W_{IR}[U] = \prod_{\lambda_j \le \tilde{\epsilon}} [1 + R_{n,\epsilon}(\lambda_j)] \; = \det(L_{n,\epsilon,\tilde{\epsilon}}[U])\;, \tag{48}$$

and a "bulk" part,

$$W_B[\eta,U] = \; \exp\left\{\eta^\dagger[1 - L_{n,\epsilon,\tilde{\epsilon}}\cdot(Q^2\cdot P_{n,\epsilon})^{-1}]\eta\right\}\;, \tag{49}$$

follows in a natural, unbiased way from the introduction of an operator which acts on pseudofermion fields and depends on $\tilde{\epsilon}$, n, ϵ and the gauge configuration U:

$$L = L_{n,\epsilon,\tilde{\epsilon}}[U] = 1 + \sum_j |\lambda_j\rangle\langle\lambda_j| R_{n,\epsilon}(\lambda_j)\theta(\tilde{\epsilon} - \lambda_j)\;. \tag{50}$$

Since the index j runs over all the eigenvalues of Q^2, the operator L, which can be diagonalised simultaneously with Q^2, has eigenvalues given by $1+R_{n,\epsilon}(\lambda_j)$ for the modes of Q^2 with $\lambda_j \leq \tilde{\epsilon}$ and by 1 otherwise. Due to the properties of the relative fit error function $R_{n,\epsilon}(\lambda) = \lambda P_{n,\epsilon}(\lambda) - 1$, the operator L is Hermitean and strictly positive, if all the λ_j's are strictly positive: a zero mode of L appears only in one–to–one correspondence with a zero mode of Q^2. In particular, the operator L has exactly the same infrared behaviour as the operator $Q^2 P_{n,\epsilon}(Q^2) = 1 + R_{n,\epsilon}(Q^2)$, if modes with $\lambda_j \leq \tilde{\epsilon}$ are present. However, because of the θ functions appearing in its definition, L is not a smooth functional of the (lattice) gauge field, in contrast with the operator $Q^2 P_{n,\epsilon}(Q^2)$.
It is then straightforward to show that eq.(49) can be rewritten in the form of eq.(33) by introducing the pseudofermion field vector $|\eta_\perp\rangle$ as in eq.(34).

B Optimizing memory requirements

We present here a general and flexible method for some optimal trading of CPU time with memory requirement in the implementation of the PHMC algorithm, which turns out to be very convenient in practical simulations.
Suppose that we wish to use the PHMC algorithm with the polynomial $P_{n,\epsilon}(Q^2)$, eq.(7), where only the degree n is relevant for the present discussion, following the implementation described in Section 2.2. Suppose also that the lattice size and the memory capacity of our computer are such that, in addition to gauge fields, their conjugate momenta and other working arrays, only $N+1$ pseudofermion fields can be stored. One of these must necessarily be the "dynamical" field ϕ extracted from the probability distribution $\exp\left[-\phi^\dagger P_{n,\epsilon}(Q^2)\phi\right]$: so we are left with the possibility of using at most N auxiliary pseudofermion fields during the evaluation of δS_P, eq.(10). Since for $N \geq n$ it is possible to use the method described in Section 2.2, we consider here only the case $N < n$, which corresponds to the situation of a relatively small storage capacity.
We have already observed in Section 2.2 that the variation δS_P, eq.(10), of the pseudofermion action S_P, is a sum of n terms. Each term depends only on two auxiliary fields, χ_{j-1}, χ_{2n-j} (and their complex conjugates), where j is the index over which the sum runs. We remark that in evaluating δS_P it is convenient to

compute first the term in the sum with $j = n$, then the one with $j = n - 1$, etc., down to the last with $j = 1$. Indeed, in this way, the auxiliary fields χ_l, with $l \geq n$ are required in the following, natural order: first χ_n, then χ_{n+1}, etc., up to χ_{2n-1}. Given this situation, the basic idea of our method is to divide the available storage space for N auxiliary pseudofermion fields into three parts:

- **(a)** A fixed storage part, where only M of the auxiliary fields $\chi_1, \ldots, \chi_n$ should be stored; let us denote them by $\chi_{i_1}, \ldots, \chi_{i_M}$.
- **(b)** A first working space part, where K pseudofermion fields can be stored; this storage space should be *large enough* to construct χ_{n-1} starting from χ_{i_M}, as well as χ_{i_m-1} starting from $\chi_{i_{m-1}}$, for all $m = 1, 2, \ldots, M-1$.
- **(c)** A second working space part, where 2 pseudofermion fields can be stored; this allows, for any given $l \geq n$, to construct and store the field χ_{l+1}, starting from the field χ_l, while keeping it stored, too.

The relation $M + K + 2 \leq N$ must of course be satisfied[4]. This relation and the above requirement about the size of the part (b) of the storage space impose restrictions on the possible choices of the integers M and K, as well as of the set of integers $\mathcal{I}_M \equiv \{i_1, i_2, \ldots, i_M\}$, satisfying $i_1 < i_2 < \ldots < i_M < n$. For the moment, let us assume that a choice of M, K and $\mathcal{I}_M$ exists which satisfies our requirements; we discuss below some examples and their practical performance. It is clear that under these assumptions the evaluation of δS_P can be performed following the strategy sketched in the steps below.

- In a preliminary step, starting from $\chi_0 \equiv \phi$, construct all the auxiliary fields χ_j, with $j \leq i_M$ and store only $\chi_{i_1}, \ldots, \chi_{i_M}$ in the sector (a).
- Set $i_{M+1} = n$, $i_0 = 0$. Then go through the following recursive procedure, where s is an integer labelling the steps of the recursion: $s = 1, 2, \ldots, M, M+1$.
- For a given value of s, let us define the auxiliary integers $p = i_{M+1-s}$ and $q = i_{M+2-s}$. Then the step s can be described as follows. Starting from χ_{i_p}

[4]We leave for the moment the freedom of using only part of the available memory, i.e. taking $M + K + 2 < N$.

construct the fields $\chi_{i_p+1}, \ldots, \chi_{i_q-1}$ and store them in the sector (b). Then evaluate the contributions to δS_P, eq.(10), with $j = i_q, i_q - 1, \ldots, i_p + 1$ (just in this order), using the sector (c) to construct and temporarily store in turn the relevant auxiliary fields $\chi_{2n-i_q}, \chi_{2n-i_q+1}, \ldots, \chi_{2n-i_p-1}$.

It may happen that only part of the sector (b) has to be used in the step with $s = M + 1$. It is also important to remark that in the steps with $s > 1$ a new evaluation of the auxiliary fields χ_j is required, for all values of $j < i_M$ and not belonging to $\mathcal{I}_M$. Indeed, these auxiliary fields were already constructed and then overwritten during the preliminary step mentioned above. The CPU time needed for their recomputation in the M steps with $s > 1$ represents the price to be paid for computing δS_P using a number of auxiliary fields less than the degree of the PHMC polynomial. On the other hand, no such recomputation occurs in the step with $s = 1$.

Let us come now to the determination of M, K, and $\mathcal{I}_M$ as functions of n and N. We recall that the chosen values of M and K must satisfy:

$$M + K + 2 \leq N \ , \qquad\qquad (M + 1)(K + 1) \geq n \ , \tag{51}$$

where the second condition is equivalent to the above requirement on the size of the part (b) of the storage space. From the description of our strategy for computing the variation of S_P, it should be clear that this condition guarantees that all of the n terms appearing in eq.(10) for δS_P can actually be evaluated. For any choice of M and K compatible with eq.(51), the set of integers $\mathcal{I}_M$ can be defined as follows:

$$i_m = n - (M - m + 1)(K + 1) \ , \qquad\qquad m = 1, 2, \ldots, M \ . \tag{52}$$

On the other hand, with respect to the simple method of Section 2.2, the computational overhead, due to the need of evaluating twice some of the auxiliary fields, is given in units of $Q\phi$ operations by:

$$C_{\text{extra}} = i_M - M = n - 1 - (K + M) \geq n - N + 1 \ . \tag{53}$$

The optimal choices of M and K are the ones which minimize C_{extra}, *i.e.* maximize $M + K$, compatibly with eq.(51): this amounts to saturating the bound $M + K + 2 \leq N$ and yields $C_{\text{extra}} = n - N + 1$. In table (7) we illustrate the performance

of this method for evaluating δS_P in some typical cases. Moreover, that table also contains results obtained by using a modified version of the method, which is useful in cases when a very limited storage space is available.

This modified version relies on the fact that it is not strictly necessary to keep constant, during the various steps of the computation of δS_P, the size of the parts (a) and (b) of the storage space. Indeed, we may only require that the parts (a) and (b) have a constant *global* size, measured by the sum $M + K$. We will see that the freedom of varying the size of the single parts (a) and (b) allows for reducing the minimal storage required for the computation of δS_P.

For instance, after the step with $s = 1$ the auxiliary field χ_{i_M} is no longer needed; which means that in the step with $s = 2$ we may take the parts (a) and (b) to have size $M - 1$ and $K + 1$, respectively. For the same reason, after each step we may decrease by one unit the size of the part (a) and increase by one unit the size of the part (b), ending with a part (b) of size $K + M$ in the step with $s = M + 1$. It is then clear that, with a suitable definition of the integers in $\mathcal{I}_M$, the computation of δS_P can be performed following exactly all the steps of our method, as explained above. Of course, the meaning of the integers M and K is now different: they only give the size of the parts (a) and (b) during the preliminary step and the step with $s = 1$.

The conditions to be fulfilled by the admissible choices of M and K, as functions of n and N, are also modified, as well as the corresponding definition of $\mathcal{I}_M$. While the condition $M + K + 2 \leq N$ remains obviously valid, the definition (52) and the second condition in eq.(51) should be replaced, respectively, by the recursive definition:

$$\begin{aligned} i_{M+1} &= n \\ i_{M+1-s} &= i_{M+2-s} - s - K \ , \qquad\qquad s = 1, 2, \ldots, M+1 \end{aligned} \tag{54}$$

$$\tag{55}$$

and by the condition

$$i_1 \leq K + M + 1 \ . \tag{56}$$

On the other hand, the computational overhead with respect to the simple method of Section 2.2 can be shown to be still given by eq.(53). As a consequence, the optimal choices of M and K are the ones that maximize the sum $M + K$ and

are compatible with the new conditions necessary for the full evaluation of δS_P. In the following we will refer to the two versions of the method presented in this section, the one with fixed size of the parts (a) and (b) of the memory and the one with variable size of the same parts, as to the basic and the modified version, respectively. The two versions are compared in table (7), for a few values of n in the range relevant for current day simulations using the PHMC algorithm. In order to give an idea of the criticality of the simulations, we also quote the typical condition number of Q^2, denoted by $k(Q^2)$, for the values of n considered.

For each value of n , we consider different values of N: the minimal one ($N = N'_{min}$) needed for using the modified version, the minimal one ($N = N_{min}$) needed for using the basic version, $N = n/2$ (in order to compare with the method of Section 5.1) and $N = n - N'_{min}$. In table (7) a prime is used to denote the quantities relative to the modified version of the computational method under study.

From table (7) we can see that the method presented in this section indeed enables one to save a significant amount of storage space at the price of a very moderate computational overhead. Namely, memory requirements are reduced by a large factor, which increases with n and is about $5 \div 9$ for the considered values of n. On the other hand, the relative computational overhead, as measured by $C_{\rm extra}/3n$, eq.(53), increases very slowly with n, approaching asymptotically the value $1/3$. It is also important to remark that these numbers refer to the maximal memory saving that can be achieved by the method. However we can see from table (7) that for each value of n many other choices of N are allowed, which correspond to a different balance between memory saving and computational efficiency. Such a flexibility makes it very easy to optimize the balance between memory saving and computational efficiency in any simulation setup, which represents a clear advantage of the method presented in this section in comparison with the ones discussed in Sections 2.2 and 5.1.

Let us come now to the comparison between the basic and the modified version of the method presented in this section. The latter version turns out to be more effective than the former in saving memory, as expected: we always find $N'_{\rm min} \leq N_{\rm min}$ in table (7), where the dots stand for cases when the basic version does not allow for a full evaluation of δS_P. However, for values of N allowed in both versions, there is no difference in the computational overhead between the

Table 7: Performance for the two versions of the method of Section 5.2 for computing δS_P, eq.(10). The notation is defined in the text: (M_0, K_0) denote, in the basic version of the method, the choice of (M, K) that minimizes, for given n and N, both $C_{\rm extra}$ and M itself. The corresponding primed quantities are relative to the modified version. Note that the minimal value of $C_{\rm extra}$ corresponding to the given values of n and N is always realized.

n	$k(Q^2)$	N	(M_0, K_0)	C_{extra}	$C_{extra}/3n$	(M_0', K_0')	C'_{extra}	$C'_{extra}/3n$
50	770	11	...	...	...	(7, 2)	40	0.267
50	770	15	(4, 9)	36	0.240	(7, 2)	40	0.240
50	770	25	(2, 21)	26	0.173	(2, 21)	26	0.173
50	770	39	(1, 36)	12	0.080	(1, 36)	12	0.080
100	1470	15	...	...	...	(11, 2)	86	0.287
100	1470	20	(9, 9)	81	0.270	(6, 12)	81	0.270
100	1470	50	(2, 46)	51	0.170	(2, 46)	51	0.170
100	1470	85	(1, 82)	16	0.053	(1, 82)	16	0.053
180	4760	20	...	...	...	(14, 4)	161	0.298
180	4760	27	(11, 14)	154	0.285	(7, 18)	154	0.285
180	4760	90	(2, 86)	91	0.169	(2, 86)	91	0.169
180	4760	160	(1, 157)	21	0.039	(1, 157)	21	0.039

two versions. Finally, we remark that for given values of n and N, there are several choices of M and K that yield the minimal overhead ($C_{\rm extra} = n - N + 1$) and are compatible with all the necessary conditions specified above. At this level, some further differences between the two versions appear, which are however irrelevant in practice. In both versions, in particular, it is not possible to choose a too small value of M, for given values of n and N, if all the necessary conditions are to be fulfilled and the minimal overhead is to be achieved: the table (7) shows also the lowest allowed values of M, and the corresponding ones of K, for the different cases.

References

[1] K.G. Wilson, Phys. Rev. D10 (1974) 2445.

[2] P. de Forcrand, Nucl. Phys. B (Proc.Suppl.) 47 (1996) 228.

[3] K. Jansen, Nucl. Phys. B (Proc.Suppl.) 53 (1997) 127.

[4] R. Frezzotti and K. Jansen, Phys. Lett. B402 (1997) 328; Nucl.Phys. B(Proc.Suppl.) 63A-C (1998) 943.

[5] P. de Forcrand and T. Takaishi, Nucl. Phys. B (Proc.Suppl.) 53 (1997) 968.

[6] M. Lüscher, Nucl. Phys. B418 (1994) 637.

[7] B. Bunk, K. Jansen, B. Jegerlehner, M. Lüscher, H. Simma and R. Sommer, Nucl. Phys. B (Proc. Suppl.) 42 (1995) 49.

[8] M. Peardon, Nucl.Phys.B (Proc.Suppl.) 42 (1995) 891.

[9] B. Jegerlehner, Nucl. Phys. B465 (1996) 487;

[10] A. Borrelli, P. de Forcrand and A. Galli, Nucl. Phys. B477 (1996) 809.

[11] A. Duncan, E. Eichten and H. Thacker, Fermilab preprint, FERMILAB-PUB-98/181-T, hep-lat/9806020.

[12] S. Duane, A. D. Kennedy, B. J. Pendleton and D. Roweth, Phys. Lett. B195 (1987) 216.

[13] K. Jansen, C. Liu, M. Lüscher, H. Simma, S. Sint, R. Sommer, P. Weisz and U. Wolff, Phys.Lett.B372 (1996) 275.

[14] K. Symanzik, "Some Topics in Quantum Field Theory", in: Mathematical problems in theoretical physics, eds. R. Schrader et. al., Lecture Notes in Physics, Vol. 153 (Springer, New York, 1982); Nucl.Phys.B226(1987)187; 205.

[15] M. Lüscher and P. Weisz, Commun. Math. Phys. 97 (1985) 59, E: Commun. Math. Phys. 98 (1985) 433.

[16] M. Lüscher, S. Sint, R. Sommer, P. Weisz, Nucl.Phys.B478 (1996) 365.

[17] M. Lüscher, S. Sint, R. Sommer, P. Weisz and U. Wolff, Nucl.Phys.B491 (1997) 232.

[18] K. Jansen and R. Sommer, Nucl. Phys. B (Proc.Suppl.) 63 (1998) 85; CERN preprint, CERN-TH/98-84, hep-lat/9803017.

[19] R. Frezzotti and K. Jansen, in preparation.

[20] M. Lüscher, R. Sommer, P. Weisz and U. Wolff, Nucl. Phys. B413 (1994) 481.

[21] S. Sint, Nucl. Phys. B421 (1994) 135.

[22] B. Sheikholeslami and R. Wohlert, Nucl. Phys. B259 (1985) 572.

[23] K. Jansen and C. Liu, Comp.Phys.Comm. 99 (1997) 221.

[24] B. Bunk, S. Elser, R. Frezzotti and K. Jansen, CERN preprint, CERN-TH/98-127, hep-lat/9805026.

[25] C. Alexandrou, A. Borici, A. Feo, Ph. de Forcrand, A. Galli, F. Jegerlehner and T. Takaishi, Nucl.Phys. (Proc.Suppl.) 63 (1998) 406.

[26] S. Gottlieb, W. Liu, D. Toussaint, R. L. Renken and R. L. Sugar, Phys. Rev. D 35 (1987) 2531.

[27] L. Fox and I. B. Parker, *Chebyshev polynomials in numerical analysis*, Oxford University Press, London, 1968.

[28] W. H. Press, S. A. Teukolsky, W. T. Vetterling and B. P. Flannery, *Numerical Recipes*, Second Edition, Cambridge University Press, Cambridge, 1992.

[29] T. Kalkreuter and H. Simma, Comp. Phys. Comm. 93 (1996) 33.

[30] I. Montvay, Comput.Phys.Commun. 109 (1998) 144.

[31] K. Jansen and C. Liu, Nucl. Phys. B453 (1995) 375.

[32] U. Glässner, S. Güsken, H. Hoeber, T. Lippert, X. Luo, G. Ritzenhöfer, K. Schilling and G. Siegert, hep-lat/9510001.

[33] R. C. Brower, T. Ivanenko, A. R. Levi and K. N. Orginos, Nucl. Phys. B484 (1997) 353.

[34] R. G. Edwards, I. Horvath and A. D. Kennedy, Nucl. Phys. B484 (1997) 375.

[35] K. Jansen and C. Liu, Nucl. Phys. B (Proc.Suppl.) 53 (1997) 974; K. Jansen, A. Jaster and C. Liu, CERN preprint, CERN-TH/97-207, hep-lat/9708017.

[36] J. C. Sexton and D. H. Weingarten, Nucl. Phys. B380 (1992) 665.